American Journal of Physics and Applications
2023; 11(3): 55-79
http://www.sciencepublishinggroup.com/j/ajpa
doi: 10.11648/j.ajpa.20231103.12
ISSN: 2330-4286 (Print); ISSN: 2330-4308 (Online)

Synchrotron Radiation X-ray Fluorescence at Grazing Incident Angle (SR-GIXRF) and Total-Reflection (SR-TXRF) of Ormosil Films Containing TiO_2 and Phosphotungstates

Orlando Elguera Ysnaga

Institute of Chemistry of Sao Carlos, University of Sao Paulo (IQSC-USP), Sao Carlos-SP, Brazil

Email address:
orlandoelguera@gmail.com

To cite this article:
Orlando Elguera Ysnaga. Synchrotron Radiation X-ray Fluorescence at Grazing Incident Angle (SR-GIXRF) and Total-Reflection (SR-TXRF) of Ormosil Films Containing TiO_2 and Phosphotungstates. *American Journal of Physics and Applications*. Vol. 11, No. 3, 2023, pp. 55-79. doi: 10.11648/j.ajpa.20231103.12

Received: April 11, 2023; **Accepted**: August 7, 2023; **Published**: September 27, 2023

Abstract: In 2011-2013 during the experiments performed at LNLS (Brazilian Synchrotron Light Laboratory) based on Grazing Incident Angle X-ray Fluorescence analysis assisted by Synchrotron Radiation (SR-GIXRF) of Ormosil (Organic Modified Silicates) films containing Phosphotungstates ($[PW_{12}O_{40}]^{3-}$) was obtained an image (Figure 8 in this article), which can be explained by different hypotheses based on physical and chemical phenomena. In 2021 the same author of this present investigation reported the possibility of to generate the conditions for the production of Maser-rays based on Total Reflection X-ray Fluorescence assisted by Synchrotron Radiation (SR-TXRF) measurements of ormosil films. Devices based on Maser-rays can extend their corresponding range of frequencies at microwave, radio, infrared, optical, ultraviolet, and X-ray regions possibly also (as was mentioned above). In this opportunity, the results of GIXRF measurements are presented. GIXRF is an XRF analysis mode in shallow incidence angles. Nonetheless, unlike of TXRF condition, GIXRF not only addresses Total Reflection phenomena, but also phenomena based on Partial Reflection (of secondary and primary X-rays), and X-ray Refraction. Thus, under these conditions, it was possible generate Molecular Fluorescence at visible region from Synchrotron Radiation X-ray Fluorescence (SR-XRF). We proposed models of Fluorescence at Molecular scale and Multiscale (from nanometer to millimeter size level) based on Luminescence phenomena, whose are result of the Interactions (physical and chemical) of Synchrotron Radiation with the matter. These Interactions can be based on the linear-polarization of relativistic electron beams generated from this X-ray source, which exhibits coherence of the rays produced. At molecular scale, the model of Fluorescence is based on the interaction of the molecular and ionic species of TiO_2 with the atomic and molecular groups of Oxygen (—O=O—) present in PWA structure, which by the chemical resonance effects of the double bonds in diene structure conjugated (.....=O—W=O—W=O—) can enable luminescence phenomena, via electronic displacements. At Multiscale level of size (result of the summation of the fluorescence model mentioned above) play an important role the Van der Waals forces, taking in consideration the contact between the great surfaces of PWA clusters and the different TiO_2 molecular and ionic species (TiO_2, $TiOH_2^+$, and TiO^-) in intramolecular and intermolecular configurations of PWA. SR-TXRF demonstrated be a suitable method for identification of Titanium and Tungsten in ormosil films.

Keywords: Synchrotron Radiation (SR), Grazing Incident Angle X-ray Fluorescence (GIXRF), Ormosil, Phosphotungstates ($[PW_{12}O_{40}]^{3-}$), Titanium Dioxide (TiO_2)

1. Introduction

1.1. Sol-Gel Process

Sol-Gel process chemistry is based on the hydrolysis, condensation, and polycondensation of molecular precursors in a "bottom-up" approach. Among the precursors, the alkoxides of the chemical elements Silicon, Aluminum, Zirconium and Titanium stand out. The monomeric metal salts such as early transition metals is considered also, in order to produce a mixture of colloidal particles ca. 2–200 nm in size dispersed in a solvent in solution (a Sol) [1]. The

advantage of Sol-Gel processing compared to the process typically employed in the ceramics industry is mainly the low processing temperatures, purity and homogeneity achieved [2]. The classic Sol-Gel reaction is the acid hydrolysis of tetraethyl orthosilicate leading to the formation of fibrous or monolithic SiO_2 [3]. During the Sol-Gel process, particles may growth without becoming crystalline, showing in X-ray crystallography line-broadening and disordered regions near the surfaces of very small crystals, which may greatly complicate detailed structural characterization. Materials made by the Sol-Gel process have a broad range of technological applications: optics, electronics, energy, space, sensing and biosensing, etc. Ormosil (organic modified silicates) are hybrid materials (combination of organic and inorganic components) prepared by Sol-Gel process that usually exhibit unique properties that traditional composites and conventional materials do not possess [4-6]. Ormosil may combine the advantages of the inorganic materials (rigidity, high thermal stability) and the organic polymers (flexibility, dielectric characteristics, ductility and ability to processing) [4-6]. The properties of ormosil can be tailored by choice of functional groups and reaction conditions, which is allowing the production of films and their corresponding properties [7]. Ormosil constitutes an adequate matrix for phosphotungstates in order to develop hybrid materials with interesting optical, mechanical, and chemical properties [8]. Phosphotungstates ($[PW_{12}O_{40}]^{3-}$ or PWA) ions can be incorporated into ormosil-based matrices by Sol-Gel method (by a bottom-up procedure) [7]. In addition, also is enable the control of matrix–PWA interactions, thus can tune the photochromic behavior of these materials [1, 7, 9-15]. PWA have potential application as acid/photo-catalysts, UV-dosimeters, due to their catalytic, photocatalytic, photochromic, and sensing properties. Polyoxometalates (POM) like phosphotungstates ($[PW_{12}O_{40}]^{3-}$) are good candidates for the preparation of such materials, because once irradiated with ultraviolet light they form colored species [7]. The photochromism of POM is based on the formation of a charge transfer complex between proton donor species, such as alkylammonium, protonated amines, and ammonium groups, and the excited phosphotungstate leading to reduced phosphotungstate species [7]. POM have well defined structures and properties and their size is typically a few nm. For this reason, POM could be considered as quantum size clusters or quantum dots. The term nanocluster sometimes is also used to refer to a nanoparticle 1 –10 nm in size. The hybrid ormosil matrices for incorporation of PWA were obtained using tetraethyl orthosilicate (TEOS) and (3-glycidyloxypropyl) trimethoxysilane (GLYMO) as matrix-forming precursors and 4-(triethoxysilyl) butyronitrile (BuTS) resulted in the formation of transparent, reproducible and uniform films. These materials are photoactive, presenting enhanced photochromic and photocatalytic behavior [15]. Ormosil studied at the present study are composed of silicates organically modified with amino (–NH_2), nitrile (–CN), diol (HO–R–R'–OH) and ether (–R–O–R'–) functionalities, which contain phosphotungstic acid ($H_3PW_{12}O_{40}.XH_2O$) and doped with Titanium oxide (TiO_2). Photochromic materials present interesting properties related to the light-induced changes in optical absorption leading to reversible coloration/discoloration upon exposure to light. The photocromism of Ormosil films can be increased by the incorporation of TiO_2 nanoparticles as was studied in our research group [1, 8-10]. Small amounts of these nanoparticles can significantly enhance the photochromic response and UV sensitivity of POMs-based hybrid materials [1, 8-10]. Titanium dioxide (Titania, TiO_2) is a colorless, stable, amphoteric crystalline solid and polymorphic. TiO_2 is present in three fundamental crystalline forms: rutile (tetragonal), anatase and brookite (both orthorhombic) [1]. Titania has found wide applications in heterogeneous catalysis and photocatalysis. A crucial characteristic of TiO_2 is the large band gap of 3.2 eV, with wavelengths below 400 nm needed to excitation, limiting the photosensitivity of Visible band of the solar spectrum [1]. The photochromic properties are important for applications as UV colorimetric dosimeters for personal protection, as well as for photochromic smart windows and lenses [1, 9, 10].

1.2. Nanomaterials Based on PWA–TiO_2 Semiconductors

The addition of heteropolyoxometallates (POMs) to TiO_2 is a successful alternative to synthesize absorbing materials at the UV-Visible light region with high photocatalytic activity, which based on the electronic features of POMs mainly. TiO_2 is a semiconductor that absorbs UV radiation, regardless of the particle sizes, which can be explained by the solid band theory. The band gap energy of the TiO_2-anatase phase is 3.2 eV, while for TiO_2-rutile phase has a value of 3.0 eV. These values of energy matches with high-energy photons in the ultraviolet region. Among the efforts made in order to expand the absorption region of TiO_2 can be mentioned: a) work with nanostructures, b) use photosensitizers, and c) introduce dopants into the structure of TiO_2. Doping and defects in the crystalline network alter the structure of bands, introducing electronic states and transitions in the prohibited bands [9]. The existence of oxygen-vacancies and impurity energy levels may be attributed to the lattice defects of TiO_2 caused by the interaction between PWA and TiO_2 [16]. Titanium dioxide (TiO_2) exhibits an excellent photocatalytic performance under mild reaction conditions with no toxicity and is a good semiconductor photocatalyst. However, electron-hole pairs tend to recombine; Polyoxometalates (POMs) are effective electron acceptors and possess photochemical properties similar to semiconductor photocatalysts, exhibiting high catalytic activity. Thus, composites based on the POMs and TiO_2 could enhance the photocatalytic activity of the catalyst (TiO_2) by increasing the electron transfer rate ($H_3PW_{12}O_{40}$ reduces the band gap energy and by the reduction of recombination rate of photogenerated carriers [17 and therein references]. PWA–TiO_2 films were successfully prepared by dipping TiO_2 nanoparticles into PWA solution, followed by thermal treatment to establish contact between clusters and TiO_2 surface [1, 9, 10, 16]. Phosphotungstic acid (PWA) clusters

modify the TiO_2 surface. Two of the most important factors that affect their photocatalytic activity are the specific surface area and crystallinity [8, 18]. Gonçalves et al studied the effect of addition of TiO_2 nanoparticles in the photochromic response of ormosil films containing PWA [10]. From visible electronic absorption spectra of TiO_2-doped ormosil–phosphotungstate films was suggested that the presence of the TiO_2 NPs enhances the photochromic response up to 277% (probably due to the transfer of photoexcited electron from the conduction band of TiO_2 to the corresponding LUMO of PWA [1, 9, 10]. Nowadays, there is no systematic study of how GAP energy influences the photochemical properties of this pair (TiO_2 and PWA), or how these two compounds interact. FTIR analysis showed small shifts of the W–O–W infrared peaks in the phosphotungstate ($[PW_{12}O_{40}]^{3-}$/PWA) suggested a possible ion-pair formation between protonated TiO_2 surface and the phosphotungstates [9, 10].

1.3. Chemical Analysis of Ormosil

A major challenge is to develop reliable methods for analyzing TiO_2 nanoparticles after they are inserted in ormosil films. Preliminary attempts for the identification/determination of TiO_2 by X-ray Diffraction and Vibrational Spectroscopy were unsuccessful. Attempts were also made by EDX with no results for Titanium. However, we were successful in determining Si and W in similar materials. One reason can be that the content of these TiO_2 nanoparticles is below the detection limit of this equipment. Therefore, it is intended to develop an appropriate analytical methodology for the determination of Titanium (Ti) in these materials. In this present study, the analysis chosen for ormosil films was XRF [8]. We performed the qualitative and semi-quantitative determination of Titanium (Ti) and Tungsten (W) in ormosil films by X-ray Fluorescence assisted by Synchrotron Radiation (SR-XRF) at modes of Total Reflection (SR-TXRF) and Grazing Angle (SR-GIXRF) [8, 10, 19, 20]. Such analysis involves the identification and determination of Titanium (Ti), at trace quantities, in order to obtain the chemical composition ratios and chemical depth profiling of thin films. X-ray fluorescence (XRF) is a high-precision method of analysis that present as advantages of to be non-destructive and need little or no preparation for the samples. XRF analysis have many applications in diverse fields: biology, medicine, environmental monitoring, geology, semiconductor industry etc. Nonetheless, XRF from laboratory is based mainly in the excitation volume of the incident X-ray beam on the sample, increasing the background scattering of X-ray, such that sensitivity to excited X-ray fluorescence is lost mainly from elements located very close to the sample surface. Thus, this method presents some limitations (detection limits of several ppm), when are necessary highly sensitive analytical methods of surface (e.g. detection limits of some ppb). One of XRF modalities that can meet these requirements is Total X-ray reflection (TXRF). TXRF is of paramount importance in atomic spectrometry [20].

1.4. Total Reflection X-ray Fluorescence (TXRF)

In 1923, the phenomenon of Total X-ray Reflection was discovered by Arthur Compton, who observed that the X-ray reflectivity in a flat sample shows a significant increase below the critical angle (0.1 ° in this case) [21]. L. G. Parratt in 1954 performed analysis of surface of solids by Total Reflection of X-rays [22]. In 1971, Yoneda and Horiuchi proposed the analysis of small amounts of Nickel (100 nanograms from a $NiCl_2$ solution) supported on optically flat substrates, being of the firsts published experiments of chemical analysis performed by Total Reflection X-Ray Fluorescence (TXRF) [23]. In 1975, Woubrauscheck and Aiginger [24] published the theoretical considerations, details of the experimental arrangement for X-ray Fluorescence in Total Reflection mode, the corresponding calibration curves and the steps in the quantification of 5µL of Chromium (Cr) and Manganese (Mn) salts in aqueous solution, reaching as detection limits of 1. 1 mg. Kg^{-1} for Cr and 2.2 mg. Kg^{-1} for Mn respectively. In 1993 Ladisich et al published the results for X-ray Fluorescence in Total Reflection mode, using a monochromatic beam and an X-ray tube with rotating anodes (Cu, Mo), reaching 170fg (1 fg = 10^{-15}g) of Mn from a standard solution [25]. TXRF is a method of analysis based on the irradiation of samples (the least possible interaction) at very shallow incidence angles on a reflective (optically flat and smooth) surface, producing a total reflection of X-rays. In TXRF, the incident radiation appears as a field of standing waves (the superposition of wide incoming and a wide reflected waves), with locally dependent oscillations or as a field of evanescent waves. TXRF depends mainly of three characteristic parameters: the critical angle, reflectivity and depth of penetration. Critical Angle is the angle corresponding to the passing through the interphase that separates the different homogeneous media, in which, the X-rays are refracted and reflected in analogously form as light. Reflectivity is defined as the ratio between the reflected and incident intensities. For angles larger than the critical angle, the reflectivity quickly tends to zero. On another hand, for angles smaller than the critical angle, the reflectivity tends to one. The low penetration depth achieved in Total Reflection condition is at the range 1-500nm, enabling the analysis of thin films/layers. TXRF is a special variation of Energy-Dispersive X-ray Fluorescence (EDXRF), but in contrast to the traditional XRF, where the primary beam strikes the sample at an angle of about 45°, TXRF uses an incident angle of less than 0.1° and the penetration depth is at the range of nanometers [25]. Due to this, the background of conventional XRF is reduced drastically, making that TXRF present low detection limits (from pg to fg levels). Among the advantages of TXRF are: 1) Self-absorption is almost negligible; 2) Detection limits are improved by the decrease of background scattering from the sample support; 3) In optical flat supports, the X-rays are almost totally reflected, because the sample is doubly excited by the

incident and reflected X-rays beams [26]. Among the characteristics that substrate must have for TXRF analysis are: flat and smooth surface, resistant to chemical attack, and hydrophobic. Quartz, Silicon, Germanium, Sapphire, and Lucite can be chosen as supports. This method has applications in traces multi-element analysis of solutions, surface analysis of solid samples, different solid sampling, among others. In addition, TXRF has applications for surface and near surface characterization, which is very useful for surface analysis of wafers, thin films, coatings among others.

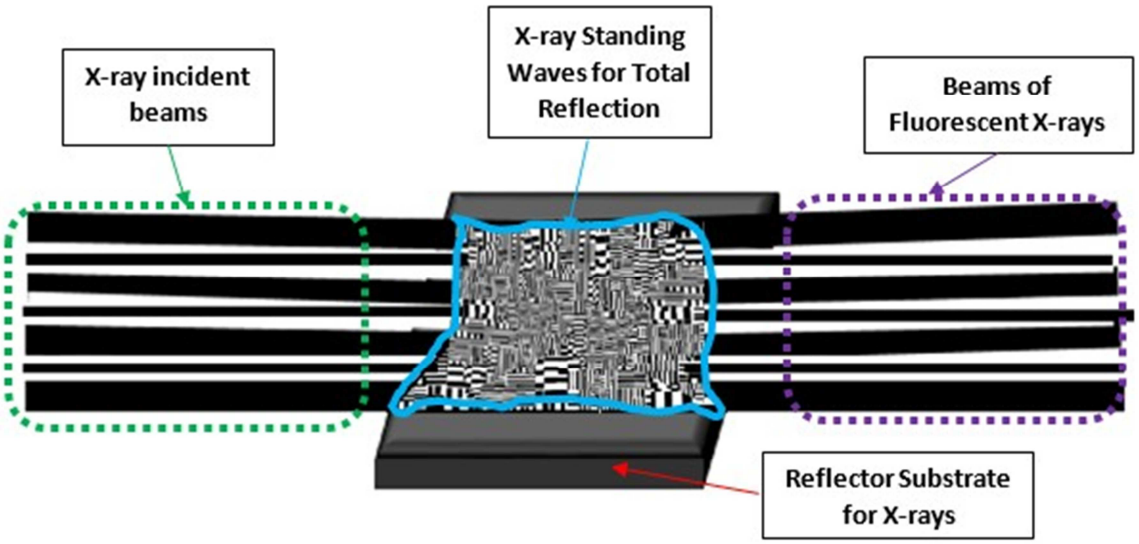

Figure 1. *TXRF Geometry.*

1.5. Grazing Incident Angle X-ray Fluorescence (GIXRF)

Grazing Incident Angle X-ray Fluorescence (GIXRF) is X-ray Fluorescence analysis in shallow incidence angles. Unlike TXRF, GIXRF not only addresses Total Reflection (in external mode) phenomena, but also Partial Reflection of X-ray Fluorescence (in external mode), X-ray Partial Internal Reflection, and X-ray Refraction. Total Internal Reflection (TIR) is the phenomenon based on the arriving of waves at the interface between two media, being completely reflected back into the "internal" medium (higher refractive index), but not refracted into the "external" medium (lower refractive index). On another hand, in Partial Internal Reflection of X-rays indeed there is not the complete Reflection, and in turn there is X-ray Refraction, which is given when the waves are refracted from a medium of higher refractive index to a medium of lower refractive index. The angle of refraction is greater than the angle of incidence, which approaching a certain threshold value, called the critical angle, the angle of refraction approaches 90°, at which the refracted ray becomes almost parallel to the boundary surface. GIXRF is the method of analysis by means of which is obtain X-ray fluorescence profile (XRF angular dependence). For example, the incident X-ray beam is recorded over a range from 0° to 2° in steps of 0.005°. The variation of the fluorescence signal as a function of the angle of incidence gives information on the distribution of excited species as a function of depth. In GIXRF the incident radiation incidence angle is adjusted between 0° and almost three times the critical angle for total reflection (of sample's-support or the corresponding layer analyzed). Below of the critical angle, it is in principle the TXRF method. Grazing angle X-ray fluorescence (GIXRF) present the features of XRF and reflectivity, constituting as a method for characterizing material layers at nanometric scale (being very sensitive even at depths of a few microns) and thin film analysis (layer thickness, interfacial profile of depth elementary, among others). This method of analysis is also used in characterization of nanoparticles deposited on flat surfaces, solar cells, and others multi-layers systems with different refractive indices [20, 26-28].

In Figure 2, at grazing angles, at shallow angles greater than the critical angle, refraction phenomena occur, due to the fact that the X-ray beam incident takes some fraction of the thickness of the support, which presents surface reflective, but roughness in its thickness. Thus, there is absorption, fluorescence, and scattering of X-rays among others phenomena (for example: reflection of X-rays without fluorescence, partial internal reflection, Auger effect, etc.). Nonetheless for our interest of analytical determination is take in consideration TXRF at the surface of the substrate and Partial XRF Reflection (in external mode) at the thickness of the substrate. In GIXRF, like in TXRF, the incident radiation appears as a field of standing waves based in this case in the superposition of narrow incoming waves and narrow partially reflected ones. Nonetheless, the standing waves produced by GIXRF would present a volume less than the volume presented by the standing waves produced by TXRF, due to that GIXRF produces other effects besides of reflection phenomena as mentioned above.

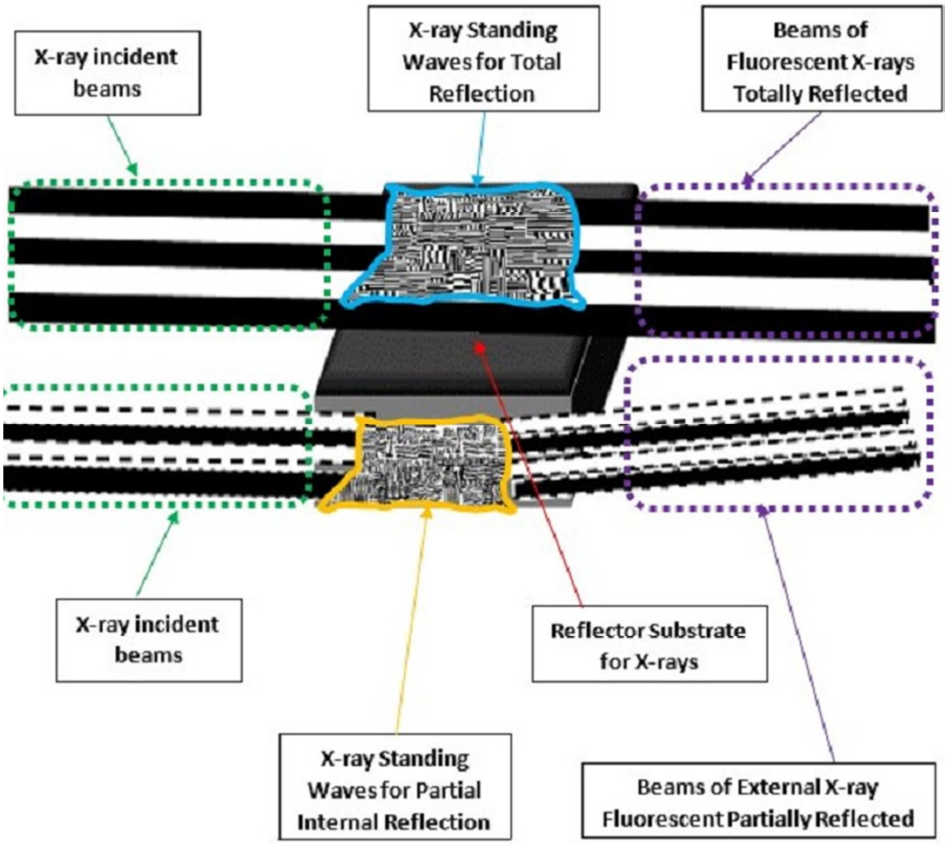

Figure 2. *GIXRF Geometry.*

1.6. Characteristics of SR-TXRF/SR-GIXRF

Synchrotron Radiation Total X-ray Reflection (SR-TXRF) has higher sensitivity than laboratory TXRF. SR-TXRF achieves the lowest detection limits due that: 1) The high spectral "brightness" of Synchrotron radiation has undergone an increase by a factor of 10^{14} compared to conventional sources, resulting in a X-ray beam primary with intensities from 5 to 15 orders of magnitude more than the obtained by X-ray tubes for TXRF analysis; 2) Synchrotron radiation is suitable for energy tuning, thus enables its adjustment in order to attain an optimum excitation for chemical elements. 3) The spectral background of SR-TXRF is further reduced than laboratory TXRF due to the polarization of synchrotron beam (100% linearly polarized in the horizontal plane of the storage ring). This last feature allows achieve detection limits three orders lower (femtograms) than obtained by conventional TXRF (picograms). SR-TXRF is especially useful in sensitive analysis of surfaces or if only small amounts of sample are available. GIXRF assisted by Synchrotron Radiation (SR-GIXRF) has the same advantages over laboratory GIXRF analogously that SR-TXRF over TXRF [20, 26-28]. In this present study, we performed the qualitative determination (identification) of Titanium (Ti) in ormosil films by X-ray Fluorescence assisted by Synchrotron Radiation (SR-XRF) at modes of Total Reflection (SR-TXRF) and Grazing Angle (SR-GIXRF) of ormosil films containing phosphotungstates doped with TiO_2 nanoparticles, aiming the correlation between the presence and localization of Titanium (as TiO_2 mainly) inside and outside of the chemical structure of these materials with their corresponding properties that exhibit. It is assumed that the substrates used as the ormosil films to be measured also presenting polished features and smoothness respectively in their corresponding top-surfaces, such that there are the suitable conditions for Reflection phenomena. Valgas de Souza in her investigation found that these films presented low average rugosity at nanometric-atomic level (0.01-1nm <> 0.1-10 Á) obtained by Atomic Force Microscopy (AFM)[1]. This range of rugosity is lower than the depth achieved under the condition of Total Reflection X-ray Fluorescence (TXRF). Thus, this method of analysis is feasible to be performed [8].

2 Experimental Section

2.1. Samples Preparation

2.1.1. Chemicals Reagents

Tetraethylorthosilicate (TEOS, 98%), 3-(glycidyloxypropyl)trimethoxysilane (GLYMO, 98%), and 4-(triethoxysilyl)butyronitrile (BUTS, 98%), Phosphotungstic acid hidrate (PWA), TiO_2 nanoparticles consisting of a 4:1 mixture of anatase and rutile (33–37 wt% in H_2O, average particle size 56 nm) were purchased from Sigma-Aldrich (USA). About the Titanium Dioxide (TiO_2) nanoparticles, a suspension of 0.1% TiO_2 nanoparticles in deionized water

(pH = 7.9) was used throughout the work, prepared from a 10% suspension (mass: volume) of TiO_2 nanoparticles (Sigma-Aldrich-USA). The suspension contains a mixture of anatase and rutile with particles with an average diameter of 50 nm according to the supplier's analysis report [5, 10]. All the reagents and solvents were used as received and without further purification. The substrates used were Silicon monocrystalline with direction [111] with area 1cm^2 and Aluminosilicate glass slides (Bioslide Technologies, USA) with area 3 cm^2 [1, 9, 10].

2.1.2. Hybrid Ormosil Films Containing Phosphotungstates Doped with TiO_2 Nanoparticles (ORMOSIL-TiO_2 (NPs)-PWA)

The detailed synthesis of these ormosil films doped with TiO_2 nanoparticles, based on the Sol–Gel method, are described on the references [5, 10, 11]. The Sol formulations used for the preparation of ormosil films are reported in Table 1; all solutions were prepared in polypropylene beakers. The general procedure for preparations of ormosil was to add the silanes (TEOS, BUTS, GLYMO) to the beakers with a micropipette and then add 25 mL of solvent mixture (ethanol/acetone 9:1) under magnetic stirring; immediately afterwards 25 mL of freshly prepared PWA solution in the mixture ethanol/acetone, which was added under magnetic stirring for 30 min. The last step consisted in adding Titanium dioxide (TiO_2) nanoparticles in suspension (0.1%m/v) with different concentrations with a micropipette [1, 9, 10]. The mixture was left under magnetic stirring for 10 min before to be deposited on substrates. Films were obtained by Dip-Coating deposition technique (WS-650, Laurell Technologies Corporation, PA, EUA), using a disc elevator MA–765 Marconi (Piracicaba, SP, Brazil) and dried under ambient atmosphere (relative humidity 45 ± 10% temperature 298 ± 3 K). The details of samples analyzed by SR-GIXRF are summarized at Table 1:

Table 1. *Details of Hybrid ormosil films containing phosphotungstates doped with TiO_2 nanoparticles (ORMOSIL-TiO_2 (NPs)-PWA) [1, 9, 10].*

Sample Code	[TEOS] 10^{-3} mol	[GLYMO] 10^{-3} mol	[BUTS] 10^{-3} mol	Volume (10^{-6}L) TiO_2 nanoparticles suspension 0.1%.	[PWA] 10^{-3} mol
SNP	9	6.8	1.5	------	0.75
A2	9	6.8	1.5	$2.0.10^1$	0.75
A6	9	6.8	1.5	$2.0.10^2$	0.75
A7	9	6.8	1.5	$1.0.10^3$	0.75
A8	9	6.8	1.5	$2.0.10^3$	0.75

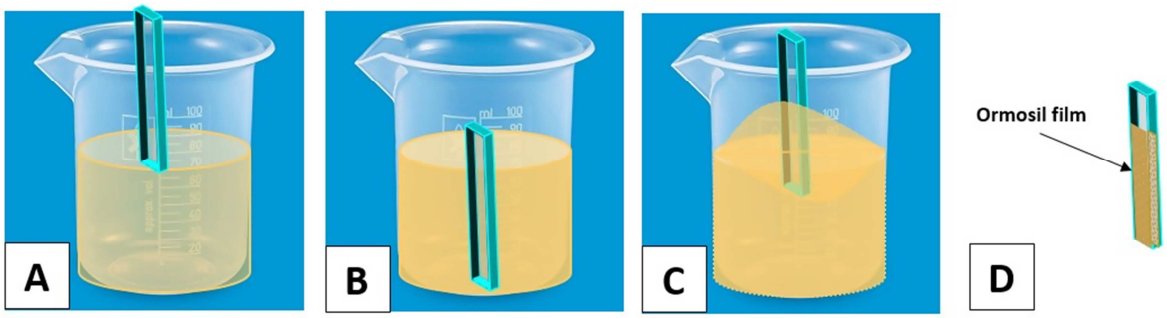

Figure 3. *Scheme showing the steps of (a) immersion, (b) adsorption-absorption, (c) emersion, (d) evaporation and drainage of the substrate in the formation of the ormosil film via Dip Coating technique.*

2.2. Instrumentation and Operational for SR-TXRF/SR-GIXRF Measurements

SR-TXRF/SR-GIXRF measurements were performed at the D09B (15°) bending-magnet XRF beamline of the Brazilian Synchrotron Light Source (LNLS, Campinas-Brazil) [28]. The experimental setup includes: 1.4 GeV source (storage ring); a monochromatic X-ray beam (dimensions: 0.1mm Vx5.0 mm H), set at 7 keV and 11keV for the determination of Titanium and Tungsten respectively; and a HPGe detector (cooled by $N_{2(g)}$) operating at energy dispersive mode. The experiments were performed at atmospheric pressure and ambient temperature. For SR-GIXRF measurements of the elements: Titanium (Ti-K_α= 4.508 keV) were not necessary any special filter arrays before of the transmission detector. For SR- GIXRF measurements of the Tungsten (W-L_α=8.396keV) was necessary a special filter array in front of the transmission detector, which consisted in 6 sets of Aluminum foils (total equivalent thickness 120 μm)[1]. For the substrates (at the energies fixed) their critical angles are at the range [0.16°-0.25°] [8]. The time of acquisition of SR-TXRF/SR- GIXRF analysis by point was 3-5 minutes approximately. For TXRF measurements, the incidence angle is fixed at just below of the critical angle of the substrate, at the corresponding energy of the X-ray beam. According to Klockenkämper [26, 27], for Silicon at 8.4 keV, the critical angle is 0.21°.

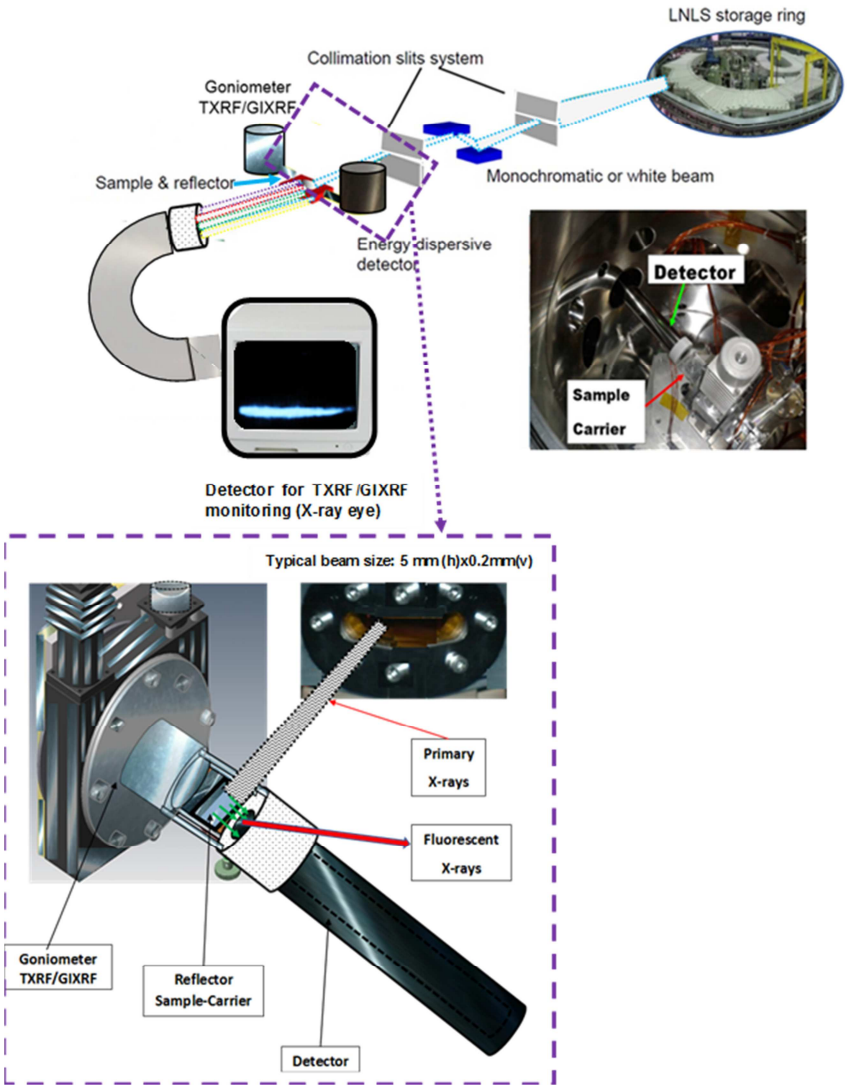

Figure 4. *Experimental set-up at LNLS for SR-TXRF/SR-GIXRF measurements.*

3. Results and Discussion

3.1. Synchrotron Radiation-Total Reflection X-ray Fluorescence (SR-TXRF): Qualitative Determinations

Between 2011-2013 during the experiments performed at LNLS (Brazilian Synchrotron Light Laboratory) was obtained the SR-TXRF Titanium spectrum of the ormosil film containing PWA doped with TiO_2 nanoparticles (A2 sample), at incidence angle of X-ray beam= 0.10°, which is shown in Figure 5:

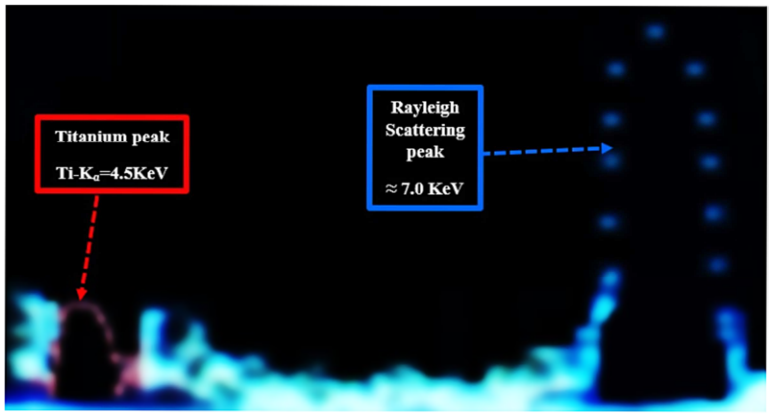

Figure 5. *SR-TXRF original Titanium spectrum of A2 sample containing PWA doped with TiO_2 nanoparticles [8].*

The treatment of SR-TXRF spectrum of the ormosil film containing PWA doped with TiO_2 nanoparticles [8] (A2 sample), at incidence angle 0.10°, by the PyMCA version 4.4[2] software, is shown in Figure 6:

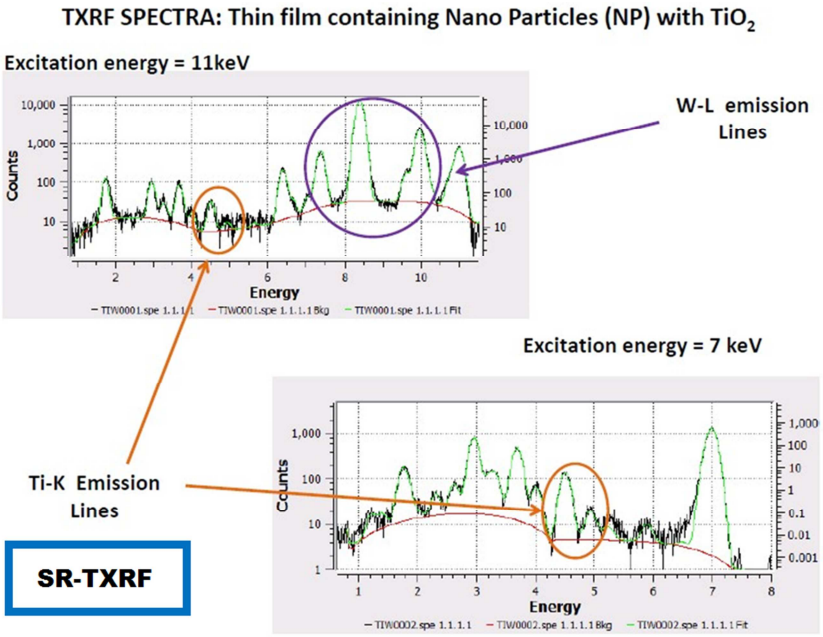

Figure 6. *SR-TXRF spectra of ormosil film A2. Top (excitation energy= 11keV for Tungsten-W determination), down (excitation energy= 7keV for Titanium -Ti determination) [8].*

Figure 6 shows X-ray peaks at 4.5 and 4.9 keV, corresponding to the XRF lines Ti-K_α (4.508 keV) and Ti-K_β (4.931 keV) [4] respectively. Analogously, X-ray peaks at 8.3 and 9.7 keV corresponding to the XRF lines W-L_α (8.396 keV) and W-L_β (9.671 keV) [8, 10] respectively. Thus, the presence of Titanium and Tungsten in the ormosil films is proved[3]. The treatment of SR-TXRF spectrum of the ormosil film containing PWA without TiO_2 nanoparticles [8] (SNP sample), at incidence angle 0.06°[4], by the PyMCA version 4.4 software, is shown in Figure 7. For the case of Silicon substrate (more used in TXRF measurements), the corresponding critical angles for the energies 11keV (for Tungsten determination) and 7keV (for Titanium determination), are 0.25 ° and 0.16 ° respectively (See Supplementary Section). From these results, we can infer that the TXRF condition can be attained at the angles range 0°-0.05°. In order to supported this hypothesis were estimated in Table A1 the critical angles. Thus, it can be inferred the presence of this element at top surface (few tenths of nanometers of depth) for these films.

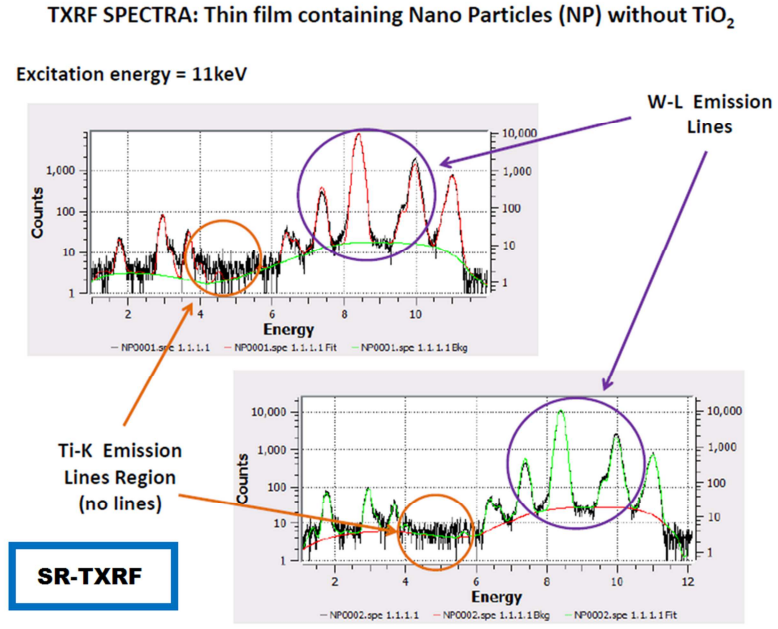

Figure 7. *SR-TXRF spectra of ormosil film SNP (excitation energy= 11keV for Tungsten-W determination) [8].*

In Figure 7 there are only the X-ray peaks corresponding to Tungsten (W-L_α: 8.396 KeV; W-L_β: 9.671 KeV) and the absence of Titanium peaks [8]. Thus, SR-TXRF demonstrates their capacity to detect Titanium in ormosil films [5]. Considering that phosphotungstate structure ($[PW_{12}O_{40}]^{3-}$) keeps intact, the presence of this anion at the ormosil films is proved [1, 8-10].

3.2. Synchrotron Radiation Grazing Angle X-ray Fluorescence (SR-GIXRF): Qualitative Determinations

In 2013, during the experiments performed at LNLS (Brazilian Synchrotron Light Laboratory) based on Grazing Incident Angle X-ray Fluorescence analysis assisted by Synchrotron radiation (SR-GIXRF) of Ormosil (Organic Modified Silicates) films containing Phosphotungstates ($[PW_{12}O_{40}]^{3-}$) was observed an image (Figure 8) that shows bluish regions (brilliant and opaque), which is different from the image obtained in 2012, during the experiments performed at LNLS based on Synchrotron Radiation-Total Reflection X-ray Fluorescence (SR-TXRF) measurements of Ormosil films containing phosphotungstates ($[PW_{12}O_{40}]^{3-}$) reported in the literature recently by Elguera et al (2021) [19].

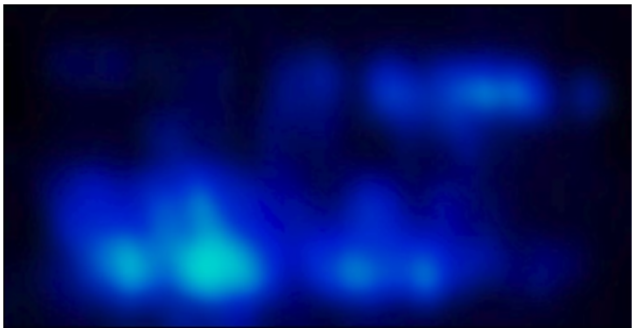

Figure 8. *SR-GIXRF condition in ormosil films (LNLS-2013) product of Fluorescence processes [8, 29].*

This image could be based partially on the interpretation of the Synchrotron Radiation Total Reflection X-ray Fluorescence analysis of ormosil films mentioned in the reference [19]. Under this condition, there would be the superposition of X-ray beams propagating unidirectionally. The brilliant beam observed in Figure 8 could be related to the intensity of Synchrotron radiation applied and the presence of phenomena based on luminescence (fluorescence, phosphorescence). Furthermore, in Grazing Incidence condition there would be X-ray scattering (reflection) and X-ray refraction (transmission). As was mentioned in the the Reference [19]. Ormosil films exhibits some degree of crystallinity at local order, maybe exhibiting polycrystalline characteristics also, which as “whole” can represent a "continuous beam" due to the summation of effects pertaining to small local crystalline domains that respond of different way to the X-ray incident beam assisted by Synchrotron radiation. According to the model presented in the Reference [19], there would in ormosil films containing phosphotungstates an electronic net of channels based on electrostatic interactions, in which the amount of Oxygen atoms of PWA play an important role. Referent to the presence of blue regions in Figure 8 there are different hypotheses:

1. In GIXRF unlike TXRF, there are more than one XSW field (at the top of the surface and also on shallow surfaces at grazing angles), where a minimum fraction of the thickness (few tens of nm) of the reflective support must be considered.

Thus, there can be destructive or constructive interferences from XSW fields, resulting in dark and bright features in image presented in Figure 8.

2. The photochromism exhibited by Phosphotungstates ($[PW_{12}O_{40}]^{-3}$) during the irradiation with Ultraviolet-light (around 260nm), which is based on the electronic transition (charge-transfer) from Oxygen to Tungsten (O(2p)→W(5d)), resulting in the heteropolyblue phosphotungstates $[PW_{12}O_{40}]^{-4}$ and $[PW_{12}O_{40}]^{-5}$ that exhibit bluish colors in the ranges 450-500 nm and 450-550nm respectively at the electromagnetic spectrum [19].

From XPS results of previous characterization of WO_3 (structural compound of $[PW_{12}O_{40}]^{-3}$), the peak located at ~4.1 eV was assigned to an O2p-derived band, while the peak centered at ~6.2 eV corresponded to a hybridized ‘W5d–O2p’ band [30]. In $WTiO_x$ films, the XPS spectra show peaks at about 3–10 eV (W5d and O2p) [31]. In the reference [1], the multielement XPS spectrum of ormosil film (obtained by our Research group) exhibit for Tungsten (W) peaks around 5–10 eV. Thus, from UV and XPS there are indicatives for the presence of the transference O(2p)→W(5d) in ormosil films.

3. The presence of Titanium dioxide with a small oxygen deficiency (TiO_{2-x}, where $x \approx 10^{-2}$), which constitutes a dark blue n-type semiconductor.

In these conditions, it could be formed the ionic specie $(TiO_{2-x}).(H_3O^+)_y.([PW_{12}O_{40+x-y}]^{-3})$, in which there would be a displacement of Oxygen atoms from Titania to Phosphotungstate [32].

4. The generation of superoxide ion (O_2^{-1}) and/or peroxide ion (O_2^{-2}) through of the reduction of phosphotungstates by the action of TiO_2 (irradiated with UV-light).
5. The generation of $(CH_2)_3(C{\equiv}N)Si(OH)_3{+}3C_2H_5OH$, as products of the hydrolysis reaction of BuTS (4-(triethoxysilyl) butyronitrile) during the preparation of ormosil samples.

This compound that contains Silicon with triple bond during the Sol-Gel process could generate oligomers and/or polymers with the structure —$[(CH)_3(C{=}N)Si(O)_3]_n$— for the sequential transference of electrons in double bonds, which in the case of alternate position (conjugated diene) are the most feasible structure, in order to generate color in the range corresponding to Visible region at the electromagnetic spectrum (when these are irradiated with UV-light).

6. There is the possibility of Fluorescence of acetylene by

photolysis process.

In the gas phase, acetylene is a principal product in the VUV photolysis of ethylene joint with diacetylene (C_4H_2 or HC≡C−C≡CH), hydrogen (atomic and/or molecular), small amounts of vinyl-acetylene (C_4H_4 or HC≡C-CH=CH_2) and benzene (C_6H_6). The photochemical primary process of acetylene initiated by absorption of light in the vacuum ultraviolet consists of (1) the formation of C_2 + H_2; (2) the production of C_2H + H; and (3) the formation of a metastable acetylene or the deactivation by collisions with the walls, inert gases, or by fluorescence. Fluorescence from C_2H_2 has recently been detected in the spectral region 2500-3500 Å. This effect observed experimentally in various acetylene clusters was termed "anomalous cage effect", which is based on the slowing down of the photofragments in inelastic collisions with the cluster constituents. The primary process is the UV photodissociation of the C–H bond resulting in formation of C_2H radical. (1) C_2H_2+hν (193 nm) →C_2H + H; (2) C_2H+hν (193 nm) →C_2 + H. There are a high number of multiphoton processes and variety of C_2H excited states. There are several secondary reactions during the photolysis of acetylene in the vacuum-UV, which can be attributed to reactions of metastable C_2H_2* molecules with C_2H_2 itself or with other reactants, producing sometimes fluorescence. Electronically, excited C_2H_2* can decompose into the following products: (a) C_2H_2*----------*C_2H +H; (b) C_2H_2*----------*C_2+ H_2; (c) C_2H_2*----------*CH+ CH. The fluorescence spectrum in comparison to the acetylene-oxygen atom flame spectrum at the same resolution of Δλ = 10 Å showed a similar apparent continuous emission starting at about 4000 Å. Among polyacetylene materials, skipped polyynes ($[–R_2X–C≡C–]_n$) are of particular and increasing interest. They consist of non-conjugated alkyne units interrupted by linker atoms (X). Nonetheless, it is possible that Silicon (Si) can enhance the interactions through of bonds and interatomic-spaces when employed as the linker atom. Thus, skipped polyynes are good candidates for functional materials such as ormosil (object of our study), semiconductors, ceramic precursors, and hole-transporting materials. The linker sp^3-atom site of skipped polyynes is able to lead to phosphorescence emissions. Furthermore, the use of a heavy atom as a linker unit (e.g. Tungsten in PWA) is expected to produce unique optical organic–inorganic polymers for functional element-block materials [33-38]. For this case, the use of a heavy atom as a linker unit is expected to produce unique optical organic–inorganic polymers for functional element-block materials. In our case the Tungsten from PWA or the same PWA as a Superatom (Ref. Elguera, 2021 [19]) can play the rol of heavy-atom as linker [39].

7. Blue Photoluminescence produced by Nanosized TiO_2 Colloids

Semiconductors as CdS, ZnS, and ZnO exhibited spectral blue-shifts in the absorption band edge as a consequence of exciton confinement caused by the so-called quantum-size effect (decrease particle size). This effect is important on the electronic, magnetic, and optical properties of semiconducting solids. Typically, the preparation of colloidal TiO_2 results in particles with diameters between approximately 5 and 20 nm. Nonetheless, it is possible quantum-size effects in very small TiO_2 colloid particles (d < 3 nm). The absorption and the corresponding bandgap energy of TiO_2 are λ_{OS}= 385 nm and E_g= 3.2 eV for anatase and λ_{OS}=415 nm and Eg=3.0 eV for rutile. A blue-shift of approximately 0.15 eV (3.35 eV or 370 nm) relative to bulk anatase TiO_2 is evident for the synthesized ultrasmall TiO_2 colloids. The photoluminescence spectrum of a dilute TiO_2 colloidal solution present important characteristics peaks: 1) At 420 nm (corresponding to bulk TiO_2 powders), 2) At 383 nm (corresponding to the blue light emitted by TiO_2). 3) At the range of 600-1000 nm, the luminescence observed is associated with transitions of electrons from the conduction band edge to holes (trapped at interstitial Ti^{3+} sites). The synthesis of TiO_2 thin films exhibiting photoluminescent and electroluminescent properties, being that the most of the luminescence observed occurs in the blue range of the visible spectrum [40, 41].

8. Generation of Superoxide Ion species

Four oxidation states of O_2 are known: $(O_2)^n$, where n is 0 (dioxygen, O_2); +1 (dioxygen cation, O_2^+); −1 (superoxide ion, $O_2^{\bullet-}$); and −2 (peroxide dianion, $O_2^{\bullet 2-}$). The monovalent reduction of O_2 gives $O_2^{\bullet-}$, which is considered both a radical (•) and an anion (charge of −1): $O_2 + e^- \rightleftarrows O_2^{\bullet-}$. The superoxide ion can be generated chemically from superoxide salts of alkali metals, and alkaline earth metals. The difficulty to overcome for superoxide ion ($O_2^{\bullet-}$) is keep in a stable state. The superoxide ion is capable of undergoing various reactions, such as disproportionation, one-electron transfer, deprotonation, and nucleophilic substitution. $O_2^{\bullet-}$ can react with various organic and inorganic substrates. Molecular oxygen in photocatalyzed reactions with TiO_2 (rutile phase) in aqueous/alcohol media produces $O_2^{\bullet-}$ as the primary product. If the reaction involves fast electron transfer between $O_2^{\cdot-}$ and $HO_2^{\bullet}$ molecules would be transferred via chemiluminescence based on the process of formation of oxygen in an electronically excited state. In TiO_2 grain surface the electrons can diffuse rapidly, forming $O_2^{\bullet-}$ with O_2 adsorbed on Ti^{3+} sites. (1) hν→ e^-+ h^+/ (2) e^-+O_2→$^{\bullet}O_2^-$. The wavelengths obtained at 375 nm and 413nm correspond for anatase and rutile respectively [42-44].

9. Mechanism based on the analogy with phenomenon of Sonoluminescence. There is possibility that the brilliant bluish lights observed in the Figure 8 can be result of luminescence caused by X-ray Standing Waves (XSW) generated in TXRF condition.

Sonoluminescence is the mechanism based on thermal and electrical theories implying the use of sound-waves in order to produce light. This mechanism is the result of the formation and /or recombination of reactive chemical species (radicals or ions) in an excited electronic state caused by the high local temperature. The emission of light excited by acoustic cavitation can be given in aqueous and non-aqueous media. Sonoluminescence can occur when a sound wave of sufficient intensity induces a gaseous cavity (through of cavitation processes) within a liquid to collapse quickly. The

sonoluminescence effect was discovered by Frenzel and Schultes (1934) based on SONAR [45], in which bubbles of the determined fluid emitted light, when the ultrasound transducer that irradiated them was turned on [46]. Spectral measurements have given bubble temperatures in the range from 2300 K to 5100 K, whose depend on experimental conditions [47]. The bubbles are very small when they emit light (at levels of μm) depending on the fluid and the gas content of the bubble. The addition of a small amount of noble gas (e.g. Helium, Argon, or Xenon) to the gas in the bubble increases the intensity of the emitted light. Peter Jarman (1960) concluded that sonoluminescence is basically thermal in origin and that it might possibly arise from micro-shocks with the collapsing cavities [48]. This phenomenon is now referred to as multi-bubble sonoluminescence (MBSL). In single-bubble sonoluminescence (SBSL), a single bubble trapped in an acoustic standing wave emits a pulse of light (presenting very stable periods and positions [49], with each compression of the bubble within the standing wave. Single-bubble sonoluminescence pulses can have very stable periods and positions [49]. If a standing acoustic wave is set up within a liquid, and the bubble will sit at a pressure anti-node of the standing wave, then a single bubble will expand and collapse over and over again in a periodic fashion, emitting a burst of light each time it collapses (between 35 and a few hundred picoseconds). Thus, under these conditions of Standing Waves, Sonoluminescence can be stable [50]. In TXRF, the processes based on X-ray Standing Waves (XSW) are of fundamental importance. In TXRF, the incident radiation appears as a field of standing waves, with locally dependent oscillations or as a field of evanescent waves. Among the ways of production of standing waves are mentioned: 1) In front of a totally reflecting surface of a thick substrate, 2) Within a thin layer on such a substrate, 3) Within a multilayer system [51]. Considering the High-intensity of the Synchrotron beam, which in turn can generate high temperatures in a short-time, there is possibility that the brilliant blue light observed in Figure 8 can be the contribution of luminescence phenomena caused by X-ray Standing Waves. According to that has been exposed, one hypothesis for the image shown in Figure 8 is that it can be the result of the presence of the X-ray Standing Waves field (XSW) produced by TXRF. One way to produce these waves is by the superimposition of an incident and a reflected wave, generating an evanescent waves field, which in our case can be carried out in an ormosil thin film layer on a Monocrystalline Silicon substrate. This field of Standing Waves interacts with the agglomerates of phosphotungstates and with different chemical species of TiO_2, causing effects of luminescence. In addition, taking in consideration that PWA distribution in ormosil films exhibit polycrystalline behavior could be given similar conditions than in the case of bubbles in liquid medium under acoustic resonance, whose can constitute sources of light. From the chemical point of view, in order to achieve luminescence (chemiluminescence), there would have to be a rupture and/or excision of chemical carbon bonds, result of the interaction of X-ray Standing Waves field with the skeleton of hydrocarbons that are constituents of the ormosil structure, generating species of the $C_2°$ type, which produces bluish lights ($C + CH_2 \rightarrow C_2° + H_2$). Another possibility is the luminescence of the TiO_2 (that emits at blue range of the visible spectrum) at nanosized scale in colloidal state (result after of Sol-Gel process of ormosil). Thus, under the experimental conditions of TXRF measurements assisted by Synchrotron Radiation of ormosil films, there are possibilities for the generation of luminescence phenomena. The Synchrotron radiation beam is essential for high energy physics experiments, which covers energies from a few eV to tens of KeV, being able to break, excise, and modify chemical bonds. Thus, the interaction of Synchrotron Radiation with matter can result in Luminescence (Thermoluminescence and Chemiluminescence) phenomena [52].

Standing Waves field (XSW) produced by TXRF.

In the next figure is presented the corresponding model of Luminescence based on the interactions of X-rays Standing Waves field (XSW) produced by TXRF with the chemical structure of PWA, taking in consideration the ausence of chemical species of TiO_2. For this case, the structure of PWA can emit bluish lights, whose could be the result of the excision of their chemical bonds by XSW interactions mentioned above.

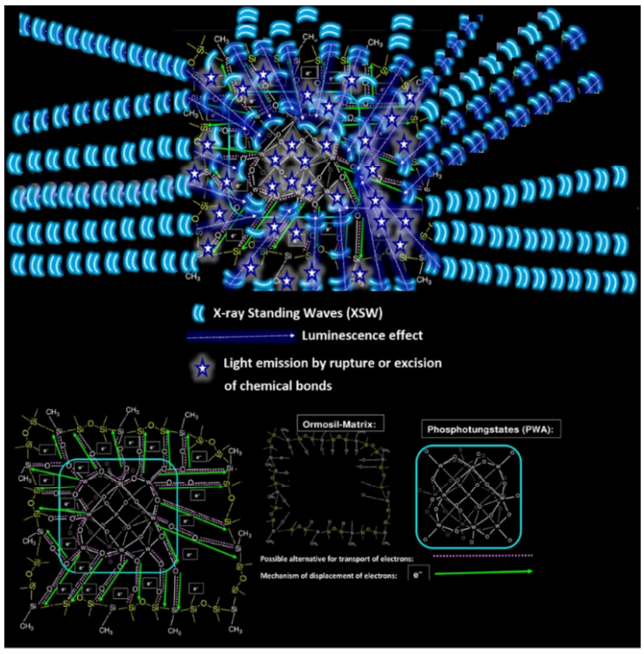

Figure 9. *Model of Luminescence of Ormosil films (containing 1 unit of PWA) without chemical species of TiO_2 based on X-rays Standing Waves field (XSW).*

In the Figure 10 is presented the corresponding model of Luminescence, taking in consideration the presence of chemical species of TiO_2, which in colloidal state at nanosized scale can emit bluish lights. Besides of this origin of these lights, It has to take in consideration the synergetic effect of the excision of the chemical bonds of PWA structure via interactions of XSW mentioned at Figure 9.

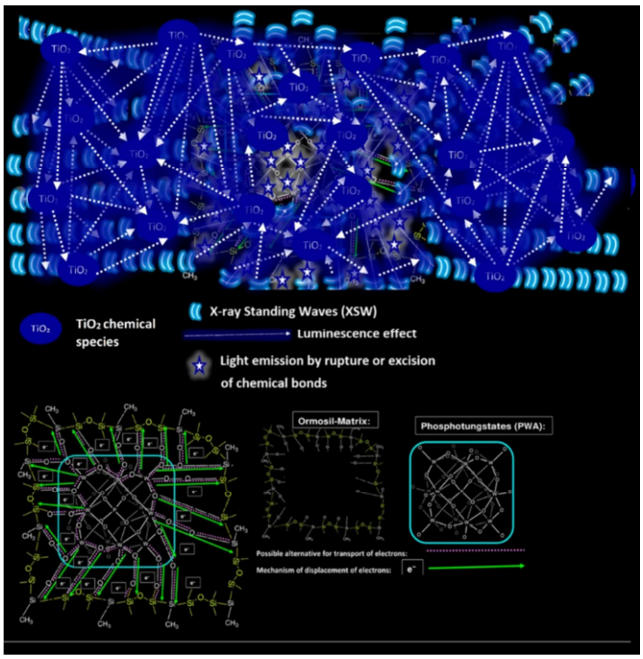

Figure 10. *Model of Luminescence of Ormosil films (containing 1 unit of PWA) containing chemical species of TiO_2 based on X-ray.*

Thus, under the experimental conditions of TXRF measurements of ormosil films, there are possibilities for the generation of luminescence by means of interaction with the evanescent waves field.

3.3. UV-Vis

In Photochemical reactions, the activation energy is supplied by the absorption of light, differently of thermochemical reactions in that the activation energy is supplied by intermolecular collisions. Upon exposure of the ormosil films to UV radiation, the photoreduction of PWA occurs, resulting in a color change from colorless to blue. This color change is reversible, and the photo-reduced phosphotungstate (heteropoly-blues species) can be gradual re-oxidized to their original colorless form (PWA) through of interactions with ambient air/O_2. The photochromic properties of the ormosil–phosphotungstate films can be studied by means of the monitoring these changes in the visible electronic absorption spectra. This remarkable increase in photochromism is probably related to the transfer of photoexcited electron from the conduction band of TiO_2 to the LUMO orbital of PWA, thereby assisting in photoreduction of PWA. The possibility that difference in photochromic response of different films may arise only from the differences of PWA content in the films is ruled out by the fact that all films have almost the same value, as measured by EDS. In order to adapt the conditions of this UV-Vis analysis to the analyzed samples mentioned in this investigation, it is detailed the equivalence of ormosil film samples in the following table:

Table 2. *Equivalence among ormosil films containing phosphotungstates doped with TiO_2 nanoparticles (ORMOSIL-TiO_2(NPs)-PWA) [1, 9, 10].*

Sample Code	Sample Code
SNP	Undoped
A2	OT-1
A6	OT-2
A7	OT-3
A8	OT-4

The photochromic behavior of PWA becomes more pronounced with increase in TiO_2 amount from OT-1 to OT-3, but falls again in case of OT-4, despite of this higher concentration. This decrease can be attributed to a "screening" or "filtering effect" caused by high loading of TiO_2. At higher TiO_2 concentration this chemical compound effectively absorbs a greater portion of UV light in the 270 nm, wavelength in which PWA absorbs also. Under such conditions, the filtering effect of TiO_2 could be more important than the charge-transfer effect in photochromic response of TiO_2-doped ormosil–phosphotungstate films. The impact of TiO_2 doping on the bleaching kinetics of the photochromic films was evaluated by monitoring, immediately after the UV exposure, the absorbance decay as function of time. The discoloration relaxation time values were evaluated by fitting the bleaching curves considering an exponential decay, as was reported by Gonçalves et al [10]. The next figure depicts the relation with the Titanium concentration was reported at supplementary information of Gonçalves et al [11], Electronic supplementary material, doi: 10.1007/s10971-015-3787-0)].

Figure 11 shows that insofar the TiO_2 concentration increase also increase the product (Absorbance x Bleaching time) up to a Titanium concentration level corresponding to the OT-3 sample (that is equivalent to A7 sample). At higher values of TiO_2 content than this level, the product (Absorbance x Bleaching time) exhibits a decrease, as in the case of OT-4 sample (that is equivalent to A8 sample). Thus, the TiO_2-doped films present slower discoloration kinetics than undoped films. This behavior may be related to the two-electron reduction of phosphotungstate leading to the formation of doubly reduced heteropolyblue species in the TiO_2-doped samples, as was reported by Gonçalves et al (2015) [10]. In this study, the TiO_2-doped films exhibited an increase up to a maximum of 277% in photochromic response compared to the undoped films, which is attributed probably to the transfer of photoexcited electron from the conduction band of TiO_2 to the lowest unoccupied molecular orbitals (LUMO) of PWA [10]. TiO_2 molecules present a low photonic efficiency (at certain conditions) for photolysis processes (based on the UV_C photon absorption) for the production of the hydroxyl radicals at its surface. At high concentrations of TiO_2 the discoloration rates are decreased, due to the reduction of photons available [53].

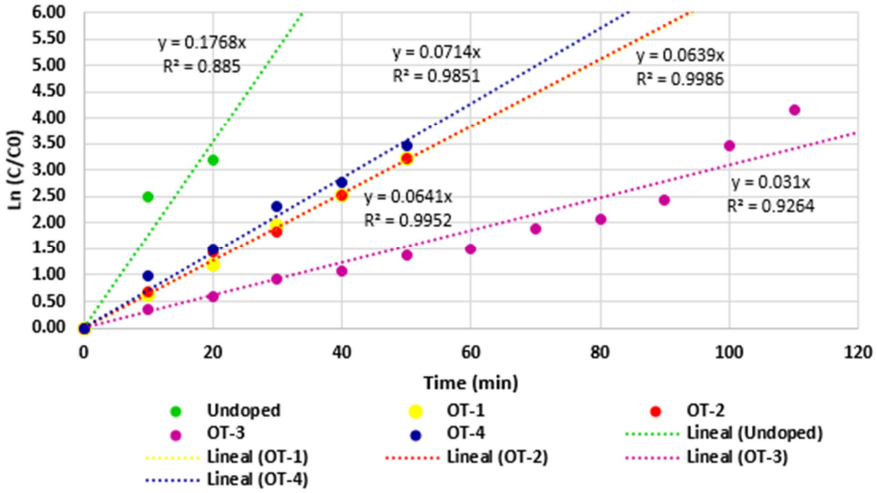

Figure 11. *Experimental and fitted absorbance decay curves for ormosil films: I) TiO_2-Undoped films: Undoped (equivalent to SNP); II) TiO_2-Doped films: OT-1 (equivalent to A2), OT-2 (equivalent to A6), OT-3 (equivalent to A7), OT-4 (equivalent to A8).*

3.4. Discussions

From these results, it can be deducted that: there is a tendency to increase the W content with the increase of the added TiO_2-NP content, indicating a possible association between these two compounds. Nonetheless, the W concentrations do not increase proportionally with the number of immersions of Dip-Coating process.

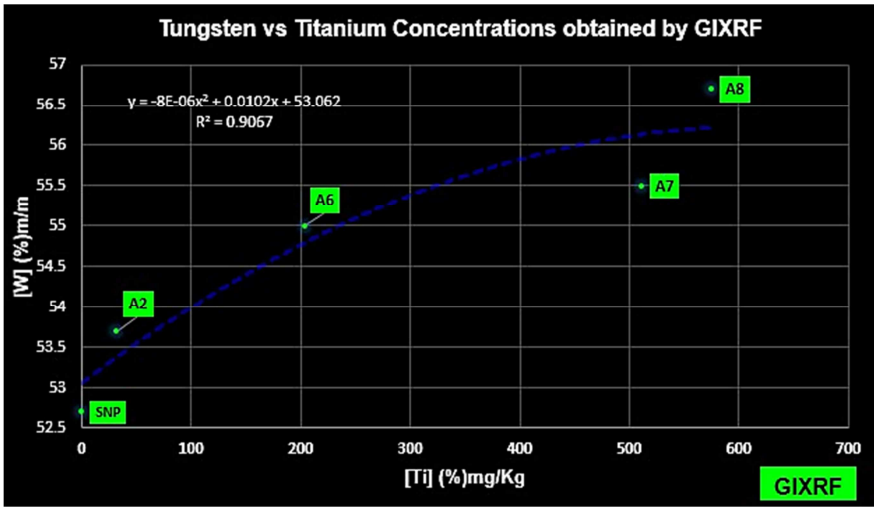

Figure 12. *Relationship of increase between Titanium and Tungsten concentrations obtained by GIXRF [8, p. 164, 184].*

The relationship of increase between Titanium and Tungsten concentrations, illustrated in the Figure 12 is only valid up concentrations of Titanium between A7 and A8 samples (around of 543 mg/Kg). At higher contents of Titanium than this average value is diminished the directly proportional relationship mentioned above [8]. This non-proportional relationship between the increase of concentrations of Titanium (from TiO_2) and Tungsten (from PWA) could be explained by the segregation of PWA clusters through the thickness of ormosil films, so that the totality of Tungsten (W) cannot be detected by method of analysis of surface as XPS and EDX. However, W can be detected by bulk method of analysis as bulk XRF and ICP-OES. This decrease of W concentration also could be based on that some of the ormosil layers did not adhere completely on substrate, insofar the number of immersions is increased, during Dip-Coating deposition technique. Another possibility is the precipitation of PWA (with or without the association of TiO_2 nanoparticles) during the preparation of colloidal suspension for ormosil films.

3.4.1. Interaction Between Polyoxometalates Molecules and Titanium Dioxide Nanoparticles

The fabrication of devices lies within the 2–200 nm size range. At 100 nm approximately, the materials stop behaving as bulk solids and instead start to show quantum effects in which the individual component can be regarded as having its own set of discrete energy levels rather than a continuous band of orbitals [52]. The boundary orbitals of phosphotungstates (around the HOMO and LUMO), have

energies and compositions similar to what is found in the orbitals corresponding to the valence and conduction bands of semiconductor TiO_2 [5]. The photochemical behavior of polyoxometalates and semiconductor oxides is based on the similarity of their spectroscopic and photochemical features, and also by their electronic structures. In fact, the polyoxometalates can be considered as quantum dots of their respective oxides. Consequently, the phosphotungstates would be the quantum dot of the mixed tungsten and phosphorus oxides. Controlling the interaction between phosphotungstate and TiO_2 can be designed more efficient photochromic materials [28]. Phosphotungstates and Titanium dioxide exhibit photoactivity due mainly to the production of -OH groups on the surface of the oxide or by adsorbed water. During the sol-gel process, the addition of H_2O lead to the hydrolysis of the silanes, which are responsible for the formation of the three-dimensional network of ormosil silicates [9].

The results of the semiquantitative determination (by methods of analysis e.g. EDXRF, WDXRF and LIBS) for the Ormosil films samples (A2, A6, A7 and A8), revealed a linear relationship between the Titanium concentration and the increase in the Tungsten concentration. This effect was justified in the hypothesis of adsorption or physisorption of Phosphotungstate ions ($[PW_{12}O_{40}]^{3-}$) on the surface of Titanium Dioxide (TiO_2) nanoparticles, constituting a "first sphere contact of Phosphotungstate ions". Steric impediments and the weak nature of the interaction of the TiO_2 + $[PW_{12}O_{40}]^{3-}$ system make it difficult for other additional Phosphotungstate ions present to be adsorbed (chemically or physically) on the surface of the TiO_2 in the same way as in this first sphere. Insofar as the precipitation effects are not important, the set of TiO_2 + Phosphotungstates nanoparticles will be mostly floating in the colloidal suspension, due to the coagulation effects, allowing their deposition on the substrate via Dip-Coating (e.g. samples A2, A6, A7). For samples with major content of TiO_2 (e.g. sample A8) the precipitation could play an important role, which would be induced by the flocculation of the colloidal system (based on the decrease in repulsive forces caused by the increase in electrolyte concentration). Furthermore, during the deposition of ormosil film (by the Dip-Coating process) the W concentrations do not increase proportionally with the number of immersions, which could be explained by the segregation of PWA clusters through the thickness of these films during the step of drying. Another possibility is the precipitation of PWA (with or without the association of TiO_2 nanoparticles) during the preparation of colloidal suspension for ormosil films. From our experimental results, which were verified by Colloid theory calculations (assuming the existence of the $TiOH_2^+$ species), it is concluded that the linear relationship between the concentrations of Tungsten (present as ($[PW_{12}O_{40}]^{3-}$)) and Titanium (present as TiO_2) is valid up to concentrations of Titanium around the nominal value corresponding to sample A8 (approx. 1.6% w/w). At higher concentrations than the corresponding to this sample, the effects of precipitation become important. In order to this hypothesis to be viable, we need a Titanium's chemical species, with a charge that helps to the solvent (e.g. ethanol) in the stabilization of this colloidal system. Huang et al [54, 8].

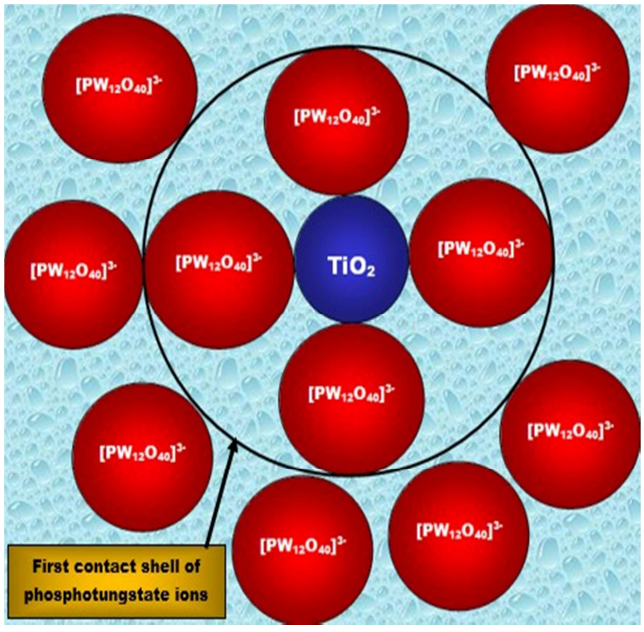

Figure 13. *Representative model of interaction between TiO_2 nanoparticles and phosphotungstates ($[PW_{12}O_{40}]^{3-}$) in organosols.*

Figure 13 illustrates that in the case of ormosil samples A2, A6, A7 and A8 would exist chemisorption or physisorption of phosphotungstate ions ($[PW_{12}O_{40}]^{3-}$) on the surface of Titania nanoparticles, possibly leading to the formation of the complex ion $\equiv Ti\text{-}OH_2^+[PW_{12}O_{40}]^{3-}$ according to published by Huang et al [54].

3.4.2. Interaction Between Polyoxometalates Molecules and Titanium Dioxide Molecules/Ionic Species

(i) *Case of Interaction between TiO_2 molecules/ionic*

species and PWA-molecular

Regarding the distribution of TiO_2 dopant—in the samples containing Titanium the maximum value determined by GIXRF is close to 1000ppm— is the fact of its molecular nature, so the interactions with polyanions as the phosphotungstates ($[PW_{12}O_{40}]^{3-}$) are weak. The larger size of the TiO_2 molecule can influence these interactions, as also is that the mobility of TiO_2 in the polyanion structure contained in ormosil is restricted, remaining the distribution of this molecule in the form of "islands". In our experiments at LNLS in 2013, we performed GIXRF measurements in order to complete the semi-quantitative analyses of Ormosil films doped with TiO_2, which could not be detected by EDX because was present in small quantity (tenths of ppm) and randomly distributed.

(ii) *Case of Interaction between TiO_2 molecules/ionic species and PWA-intramolecular*

In order to determine the possibility of interactions between TiO_2 molecules and the interior of PWA-cage structure is necessary the knowledge of the size of both molecules. If the size of TiO_2 molecule is lower than the corresponding interatomic distance within the PWA-cage structure, which can host this molecule, then intramolecular interactions will be feasible. PWA clusters (spherical structure) can achieve a diameter from 20–25 nm and TiO_2 crystal size is 8.3nm. Thus, there are conditions for these molecular/ionic interactions. Among the intramolecular interactions can be mentioned:

Considering that the TiO_2 molecule that interacts with the PWA-intramolecular structure exhibit non-polar characteristics, it is going required a non-polar solvent in order to keep present the interactions mentioned above. For example, for this case there would be present London's Dispersion forces.

If there are ionic species of TiO_2 (e.g. $TiOH_2^+$), considering the distribution of electrons in ormosil structure, according to the model proposed by Elguera et al (2021) [19], there are some possibilities of polar interaction with a solvent like ethanol (or others of polar nature), which are used in ormosil preparation.

(iii) *Case of Interaction between TiO_2 molecules/ionic species and PWA-intermolecular*

If the size of TiO_2 molecule is higher than the corresponding interatomic distance within the PWA-cage structure, which cannot host this molecule, then intermolecular interactions be more feasible than intramolecular interactions. Among the intermolecular interactions can be mentioned:

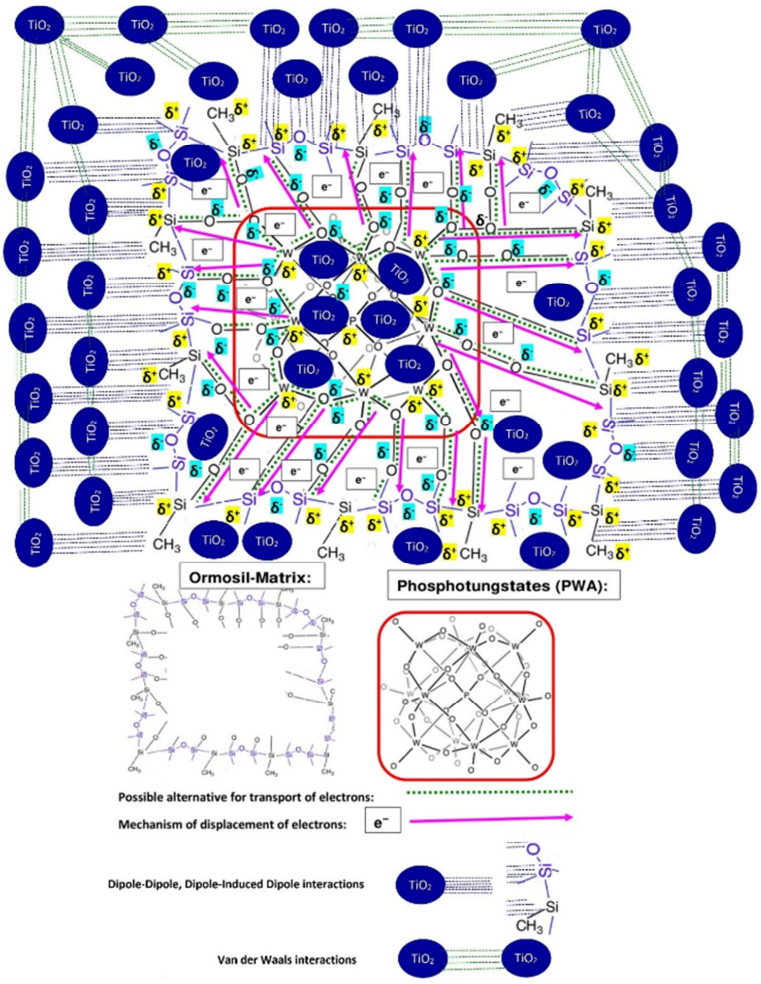

Figure 14. *Interaction between TiO_2 molecules and PWA-intramolecular/Interaction between TiO_2 molecules and PWA-intermolecular: Dipole-Dipole type. Van der Waals forces among the same TiO_2 molecules.*

1. *Dipole-Dipole type*: The structure of ormosil corresponds to the Materials Class-II, where the covalent bond is predominant. For this reason, this type of force is important if the TiO_2 molecules have the function of "bridge" between the ormosil structure and the PWA clusters occluded in this one, as is shown in Figure 14.
2. *Ion-Ion type*: These electrostatic forces are feasible in the case of interactions between ionic species of TiO_2 e.g. $TiOH_2^+$, TiO^- and the negative and positive charges of PWA-clusters, as are shown in Figures 15, 16 and 17.
3. *Ion-Dipole type*: There are possibilities for these forces in the case of ionic species of TiO_2 e.g. $TiOH_2^+$, $TiO^-$and similar others, which interacting with the polar molecular species constituent ormosil and PWA structures. as are shown in Figures 15 and 16.
4. *Dipole-Induced Dipole type*: This force is important among the TiO_2 molecules, as is shown in Figure 14.
5. *Van der Waals type*: these forces are present among TiO_2 molecules.

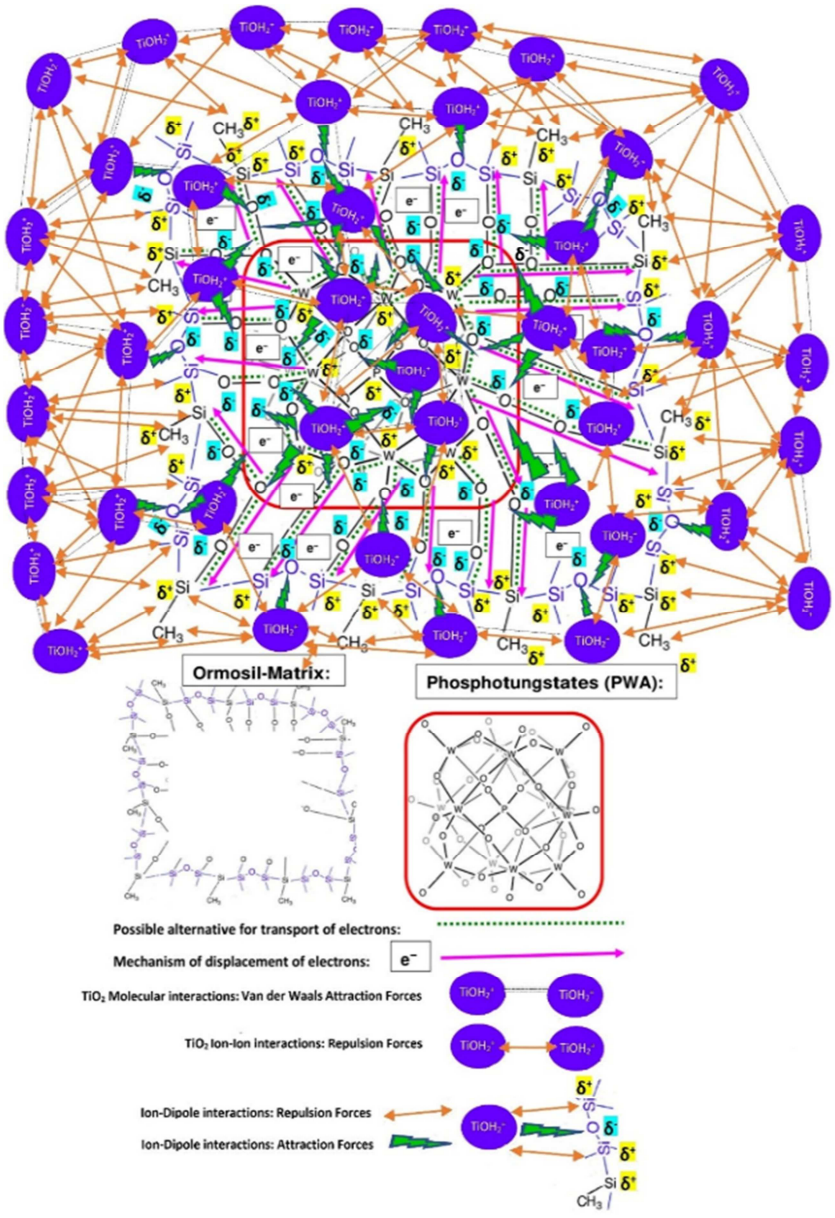

Figure 15. *Interaction between TiO_2 ionic species ($TiOH_2^+$) and PWA-intramolecular/ Interaction between TiO_2 ionic species ($TiOH_2^+$) and PWA-intermolecular: Ion-Dipole type.*

Among PWA molecules would be feasible the intermolecular interactions, when the distances between neighboring ones are less than 17.0 Å [55]. The capacity of PWA to form clusters and the number of these can result in a high surface in order to generate the necessary conditions for the existence of Van der Waals forces, as is shown in Figure 14 for TiO_2 molecules. PWA clusters can also present behaving of crystal structure, exhibiting high-capacity of

amplification of generation of electrons. According to the Reference [19], this intermolecular mechanism can be similar with the observed in one photomultiplier tube, which emits electrons when photons of adequate frequency strike it. The interaction of Synchrotron X-ray with PWA molecules can generate radiative processes (photoelectric effect, electroluminescence), as also non-radiative processes (e.g. Auger Effect). The negative charge of PWA significantly increases the opposite positive charge accumulated on Silicon compounds at surface and channels at bulk level in Ormosil films via electrostatic interactions [56, 57]. In the following Ormosil structure containing PWA, the TiO_2 molecules distribution are interacting mainly by Van der Waals, and Dipole-Dipole forces (δ^+, δ^-).

In the following Ormosil structure containing PWA, the $TiOH_2^+$ ions distribution are interacting mainly by Electrostatic forces, Dipole-Dipole interaction, Ion-Dipole attraction forces ($TiOH_2^+$-----δ^-), and Ion-Dipole repulsion forces ($TiOH_2^+$-----δ^+); and among $TiOH_2^+$ ions interacting mainly by Electrostatic, Dipole-Dipole (δ^+, δ^-) and Van der Waals forces.

In the following Ormosil structure containing PWA, the TiO^- ions distribution interacts mainly by Ion-Dipole attraction (TiO^------δ^+) and Ion-Dipole repulsion forces (TiO^------δ^-); and among TiO^- ions interacting mainly by Electrostatic, Dipole-Dipole (δ^+, δ^-) and Van der Waals forces.

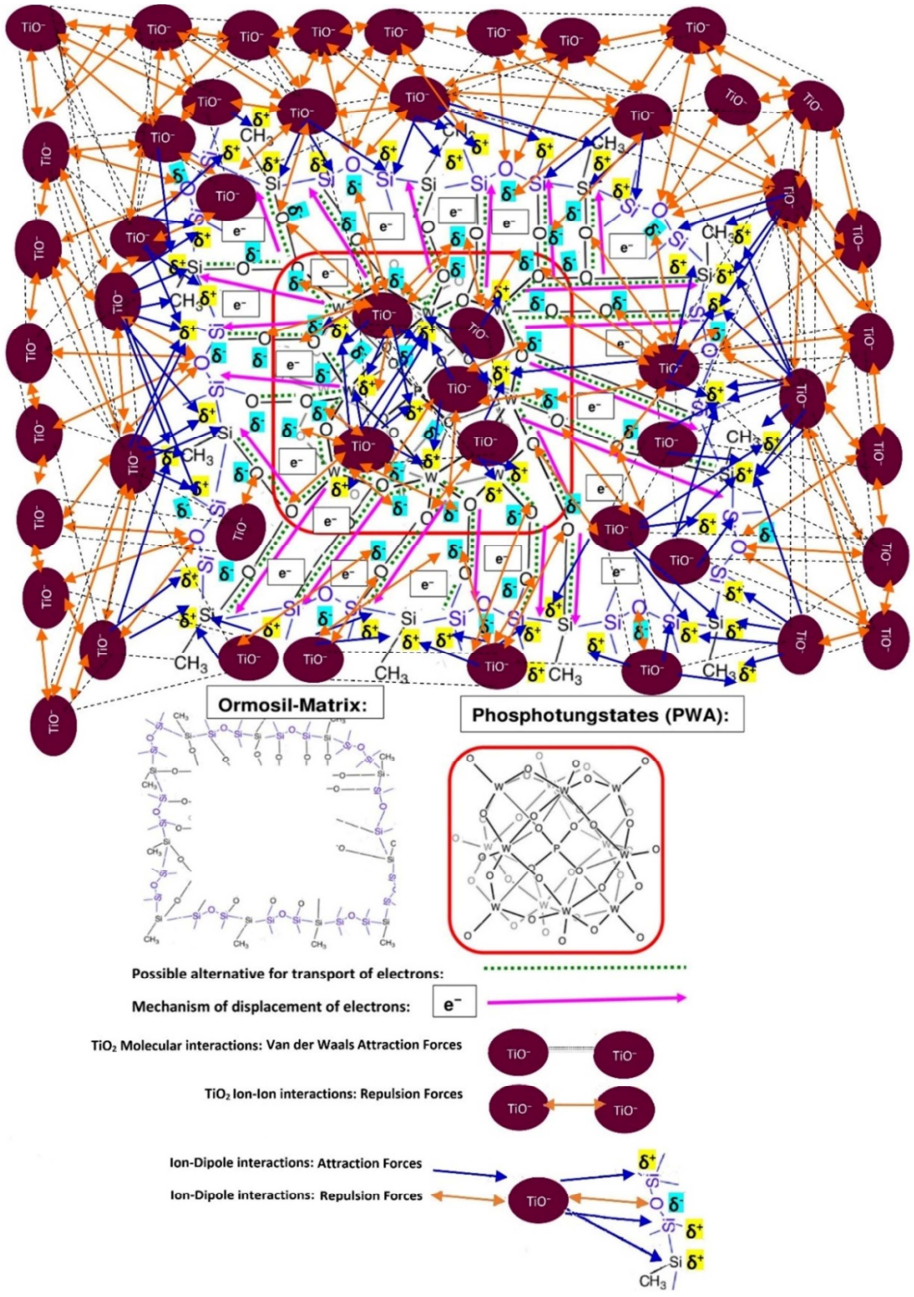

Figure 16. *Interaction between TiO_2 ionic species (TiO^-) and PWA-intramolecular/ Interaction between TiO_2 ionic species (TiO^-) and PWA-intermolecular: Ion-Dipole type.*

For $TiOH_2^+$ and TiO^- ions Van der Waals forces (contact forces) have been considered, in order to explain their interactions at surface level, assuming that the charge distribution at surface and bulk level of the ions derived from TiO_2 do not present a homogeneous density of charge. Thus, the electrical charge suits better as a distribution of charge than a point charge.

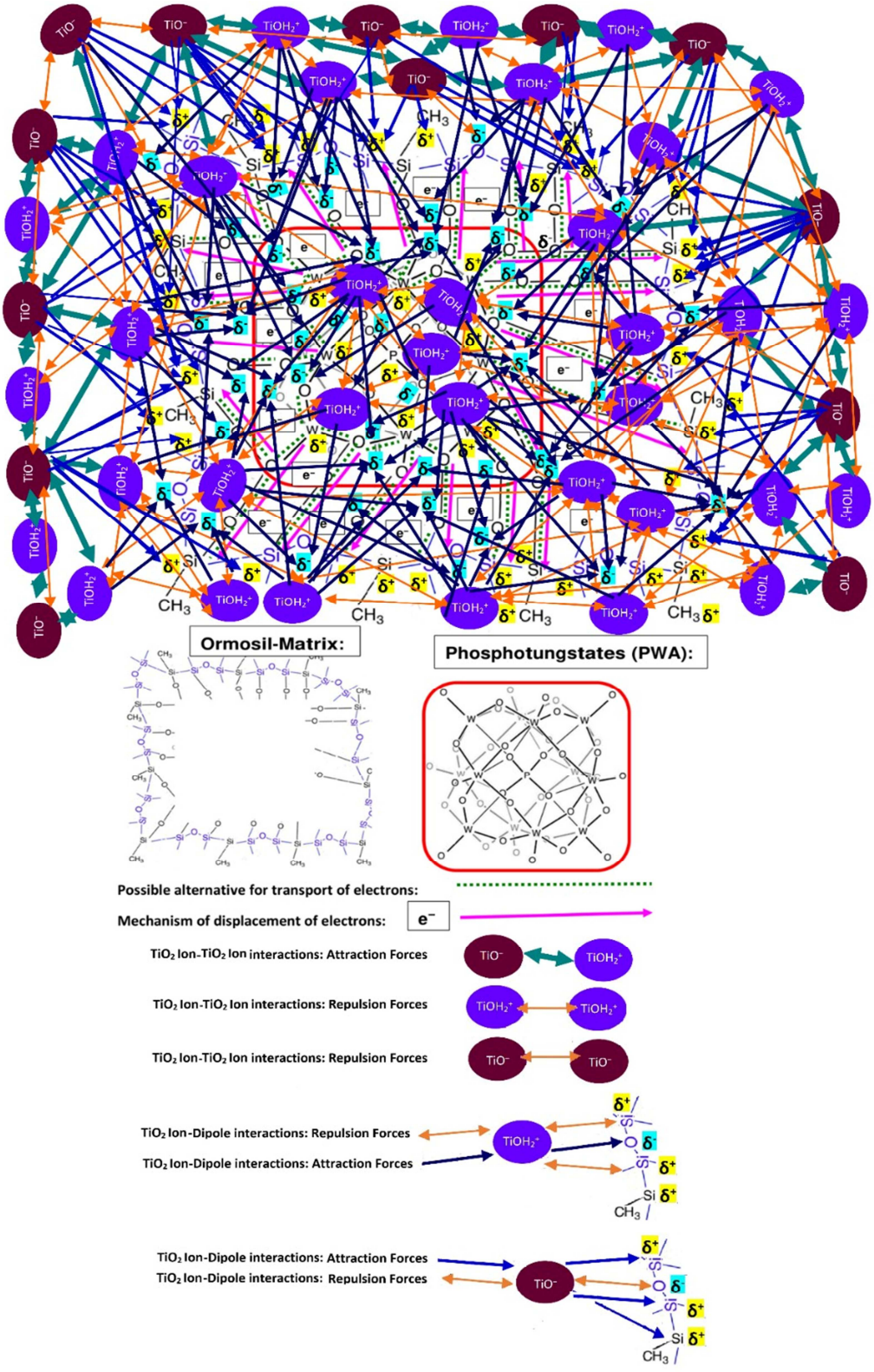

Figure 17. *Interaction between TiO_2 ionic species ($TiOH_2^+$) and PWA-intramolecular/ Interaction between TiO_2 ionic species ($TiOH_2^+$ and TiO^-) and PWA-intermolecular: Ion-Dipole type and Electrostatic forces (attraction and repulsion).*

3.4.3. Fluorescence Models for Interactions Between TiO_2 and PWA Species

In 2021 Elguera et al reported the possibility of generate the conditions for the production of Maser-rays based on Total Reflection X-ray Fluorescence assisted by Synchrotron Radiation (SR-TXRF) measurements of ormosil films. Maser-rays constitute devices that generate electromagnetic waves, which can extending their corresponding frequencies range at microwave, radio, infrared, optical, ultraviolet and X-ray regions. Thus, from the point of view of Fluorescence phenomena, it was possible generate Molecular Fluorescence at visible region from Synchrotron Radiation X-ray Fluorescence (SR-XRF). Maser can constitute systems of spontaneous emission, capable of producing coherent amplification at very high frequencies. For example, at Ultraviolet region and higher frequencies is necessary a very monochromatic radiation and the use of highly reflecting surfaces. Thus, Synchrotron Radiation-Total Reflection X-ray Fluorescence (SR-TXRF) measurements in ormosil films can generate the conditions for production of maser rays due to: 1) The coherence that X-rays exhibit (produced by quantum fluctuations), 2) The ability for energy tuning along the electromagnetic spectrum (wide range of wavelengths/frequencies), 3) The features that X-ray beam applied possess: monochromaticity, polarizability and brilliance. For Total Reflection X-ray Fluorescence (TXRF) analysis is crucial that the surfaces used be reflectors. Besides of the Synchrotron X-ray beam characteristics, there is possibility of phenomena based on luminescence (fluorescence and phosphorescence). In wavelength ranges corresponding to Ultraviolet region, the Phosphotungstates exhibit very interesting phenomena as the photocromism that occurs when the irradiation is performed at around 260nm. This irradiation involving electronic transitions (e.g. O(2p) →W(5d)) within the boundary orbitals of phosphotungstate, which as reduced specie ($[PW_{12}O_{40}]^{-4}$) exhibit a bluish color (called heteropolyblue), which disappears in the presence of oxygen. Furthermore, due to the multiples multi-electronic collisions present in phosphotungstates, it is probable found photoluminescence effects also. Under these conditions, there is viability to develop Molecular Fluorescence from SR-TXRF of Phosphotungstates contained in Ormosil structure, based in the generation of Maser-rays.

From the possible interactions between TiO_2 and PWA species, We have proposed models of Fluorescence at Molecular scale and Multiscale (from nanometer to millimeter size level), in order to support the basis of Luminescence phenomena (result from the interactions of Synchrotron Radiation with ormosil films) manisfeted in the image observed in Figure 8 under GIXRF condition:

(i) *Fluorescence model at molecular scale level of size between TiO_2 molecular-ionic species ($TiOH_2^+$ and TiO^-) and PWA-intramolecular and PWA-intermolecular chemical structures.*

For ormosil films the pathways of electron transfer of Phosphotungstates (PWA) could be internal (inside isolated and non-isolated PWA molecules) and external (among PWA molecules and their surroundings). Due to the Luminescence (Phosphorescence and Fluorescence) and Thermoluminescence obtained from Interactions of Synchrotron Radiation with the matter, we have proposed models of Fluorescence at molecular scale and Multiscale (from nanometer to millimeter size level). The following model is based on the interaction of the molecular and ionic species of TiO_2 with the atomic and molecular groups of Oxygen (—O=O—) that through the double bonds with the Tungsten atoms (—W=O—) in Phosphotungstates (PWA), it is configuring an chemical structure resonant that enables luminescence phenomena, via the electronic displacements of these double bonds (.....—W=O—W=O—W=O—O—W— O=W—O—O—W—.....), as mentioned by Elguera et al 2020 [19]. The ionizing radiation from the Synchrotron can sustained these models of fluorescence due to the coherence exhibited (based on Quantum fluctuations) and by the linear-polarization of their relativistic electron beams [58]. Among PWA molecules and Ormosil matrix it is possible the chemical resonance between Oxygen bonds (—O—O—), in order to form temporally chemical bonds as —Si—O—O— conducting the electrons outside of the Phosphotungstate structure and surroundings based on the high electronegativity of Oxygen atoms [56, 57].

(ii) *Fluorescence model at Multiscale level of size between TiO_2 molecular-ionic species ($TiOH_2^+$ and TiO^-) and PWA-intramolecular and PWA-intermolecular chemical structures.*

For this model, it is taken in consideration that in the study of TiO_2 nanoparticles (up to micro-level) their surface can be negative or positive based on the following equilibria: $TiOH + H^+ \rightarrow TiOH_2^+$/ $TiOH + OH^- \rightarrow TiO^- + H_2O$ (7). Synthesis of blue Titania with Ti^{3+} localized in the core of TiO_{2-x} nanoparticles [17]. The interactions of Synchrotron Radiation with the matter can be manifested as Luminescence (Phosphorescence and Fluorescence) and Thermoluminescence. In this multi-model is considered the summation of the conditions of the fluorescence model of Figure 18 from molecular level (corresponding to the PWA individual structure) up to millimeter level. For this case, Van der Waals forces play an important role due to the contact between the great surfaces (when compared at the typic molecular size scale) of the agglomerates corresponding to the molecular arrays of Phosphotungstates interacting with the different TiO_2 molecular and ionic species (TiO_2, $TiOH_2^+$, and TiO^-) at chemical structures of ormosil occluding PWA (at intramolecular and intermolecular configurations).

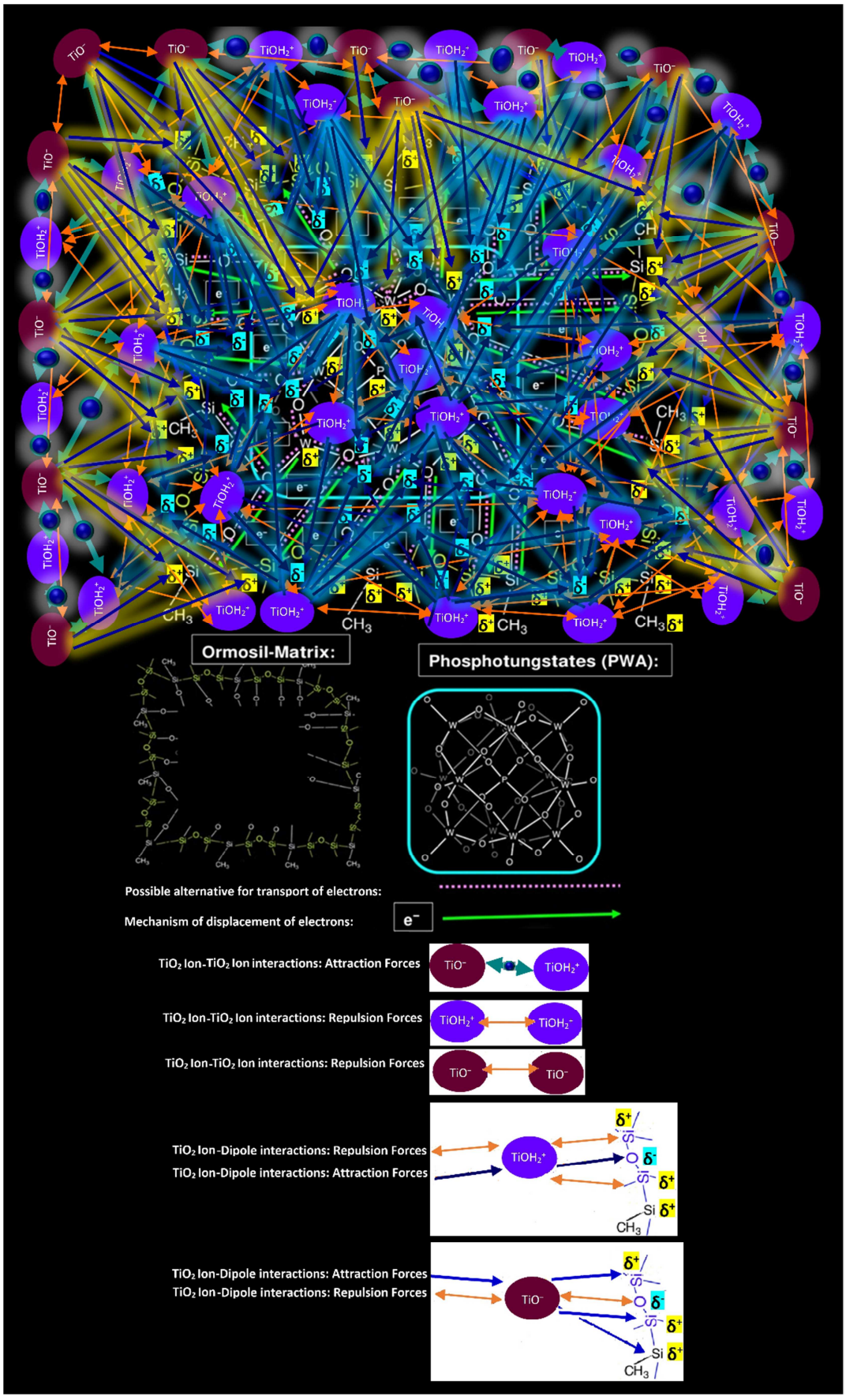

Figure 18. *Fluorescence model based on the Interaction (Ion-Dipole type and Electrostatic forces) between TiO_2 ionic species ($TiOH_2^+$ and TiO^-) and PWA-intramolecular and PWA-intermolecular chemical structures.*

$$PWA_i^{-1} = PWA_i + TiO_i^- \quad (1)$$

$$PWA_i^0 = PWA_i + {TiO_2}_i^0 \quad (2)$$

$$PWA_i^{+1} = PWA_i + {TiOH_2}_i^+ \quad (3)$$

$$\text{Cluster } PWA^{-1} = \sum_1^n PWA_i^{-1} \quad (4)$$

$$\text{Cluster } PWA^0 = \sum_1^n PWA_i^0 \quad (5)$$

$$\text{Cluster } PWA^{+1} = \sum_1^n PWA_i^{+1} \quad (6)$$

Where $PWA_i^{-1}, PWA_i^0, PWA_i^{+1}$, corresponding to the molecular arrays of Phosphotungstates PWA , in which TiO_i^- (anion), ${TiO_2}_i^0$ (molecular), ${TiOH_2}_i^+$ (cation) are keep positioned inside and/or outside of these chemical structures through multiple interactions from different origins.

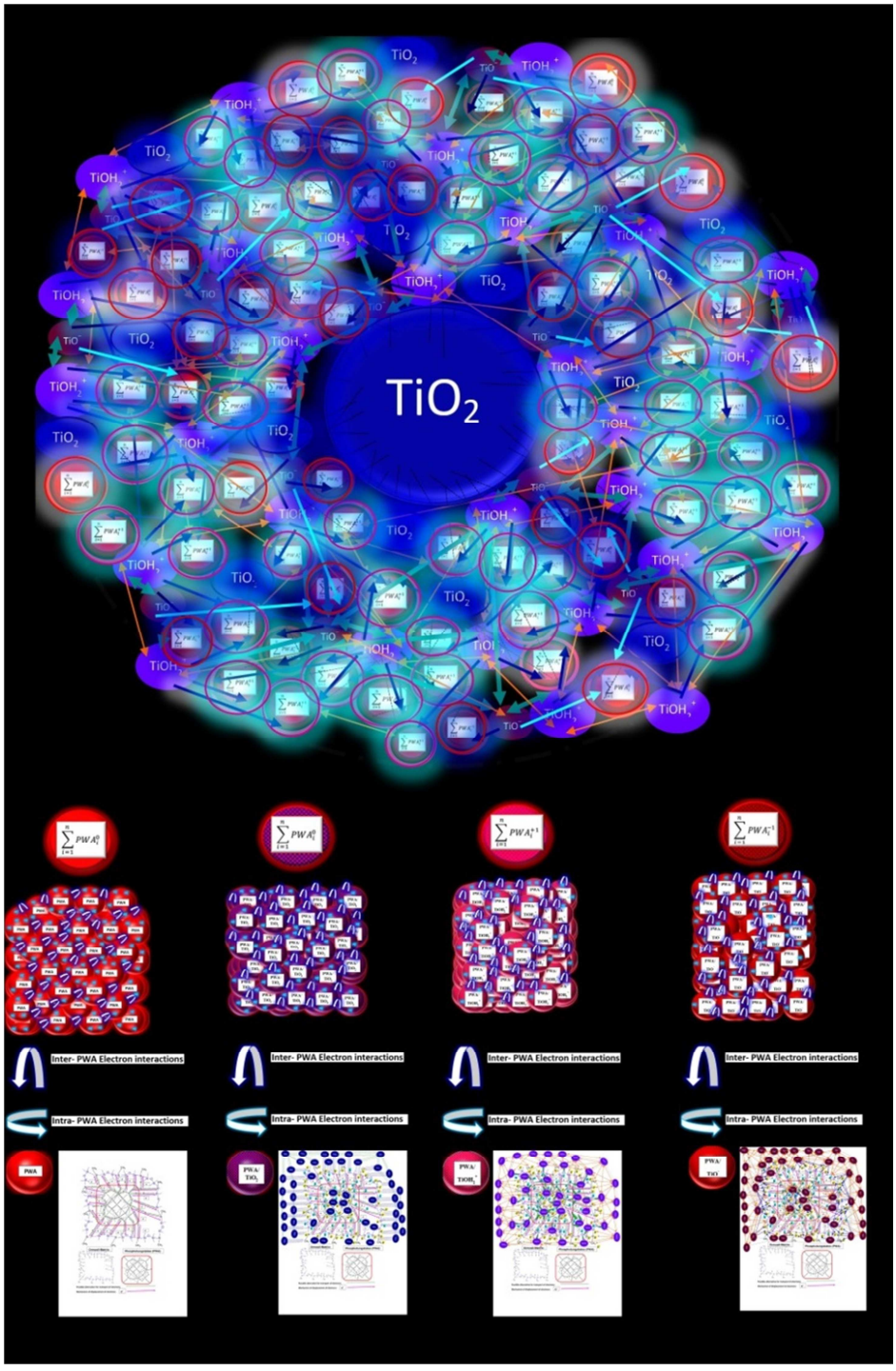

Figure 19. *Fluorescence model based on the Interaction Ion-Dipole type, Electrostatic forces, Van der Waals forces) at Multiscale level of size between TiO_2 ionic species ($TiOH_2^+$ and TiO^-) and PWA-intramolecular and PWA-intermolecular chemical structures.*

4. Conclusions

Between 2011-2013, during the experiments performed at LNLS based on Grazing Incident Angle X-ray Fluorescence analysis assisted by Synchrotron Radiation (SR-GIXRF) of Ormosil films containing Phosphotungstates ($[PW_{12}O_{40}]^{3-}$) was observed an image depicted at Figure 8, which can be explained by different hypotheses based on physical and chemical phenomena. Grazing Incident Angle X-ray Fluorescence (GIXRF) is a X-ray Fluorescence analysis in shallow incidence angles. Unlike TXRF, GIXRF not only addresses Total Reflection phenomena, but also Partial Reflection of X-ray Fluorescence and X-rays, and X-ray Refraction. SR-GIXRF and SR-TXRF are suitable methods of analysis for qualitative determination of Titanium and Tungsten in ormosil films. We have proposed models of Fluorescence at Molecular scale and Multiscale (from nanometer to millimeter size level), in order to support the basis of Luminescence phenomena (result from the interactions of Synchrotron Radiation with ormosil films) manisfeted in the image mentioned above under GIXRF condition. These models are based on the coherence and linear-polarization exhibited by relativistic electron beams inside of Synchrotron ring. At molecular scale, the model of Fluorescence is based on the interaction of the molecular and ionic species of TiO_2 with the atomic (—O—) and molecular groups (—O=O—) of Oxygen present in PWA structure, conforming the chemical structure (.....—W=O—W=O—W=O—O—W—O=W—O—O— W—.....) that by the chemical resonance effects of the double bonds in diene structure conjugated (.....=O—W=O—W=O—) can enable luminescence phenomena, via their electronic displacements. For ormosil films, the pathways of electron transfer of Phosphotungstates (PWA) could be internal (inside of the isolated PWA molecules, and non-isolated PWA molecules) and external (among PWA molecules and their surroundings). At Multiscale level of size (in this multi-model is considered the summation of the fluorescence model of Figure 18) play an important role the Van der Waals forces, taking in consideration the contact between the great surfaces of the agglomerates corresponding to the molecular arrays of Phosphotungstates occluded in ormosil structures interacting with different TiO_2 molecular and ionic species (TiO_2, $TiOH_2^+$, and TiO^-) at intramolecular and intermolecular configurations of PWA.

Acknowledgments

The author thanks to the São Paulo Research Foundation (FAPESP) by the research grants (2011/08120-0, 2011/06019-0, 2013/05279-3) and to the CNPq Brazilian agency by the financial support (research grants 141880/2011-2 and 160515/2011-4). We also extend our gratitude to the Dr. Carlos Perez for his help at the SR-TXRF/SR-GRXRF measurements done at Brazilian Synchrotron Light Source (LNLS), to the CNPEM-LNLS facilities for SR-TXRF/SR-GRXRF measurements (proposal numbers: XRF-14217, XAFS1-14254 respectively). Furthermore, the author wish expresses his gratitude and acknowledgement to Prof. Dr. Jun Kawai (Department of Materials Science and Engineering- Kyoto University) by his help and advices. Finally, the author thanks to the Jean-Jacques Pireaux des Facultes Universitaires Notre Dame de la Paix (Namur, Belgium) for the use of Winspec 2.0 and to the Inorganic Hybrid Materials Chemistry Group (IQSC-USP), São Carlos, São Paulo-Brazil.

Appendix

For the case of the Silicon substrate, with atomic number (Z), atomic mass (A) and density (ρ) keeping constant, the value of critical angle will depend only on the energy of the X-ray beam. To calculate the critical angle from a known value, the following equation is obtained:

$$\alpha_{c_1} = \left(\frac{E_1}{E_2}\right) * \alpha_{c_2}$$

α_{c_1}: Critical angle (°) in energy E_1
α_{c_2}: Critical angle (°) in energy E_2
E_1, E_2: X-ray beam energies (keV)

Table A1. *Depth of analysis and Critical Angle as function of X-ray beam energy.*

Beam Energy (keV)	Critical Angle (α_c °)	Depth of analysis Z_n (nm)
7.0	0.25	27
8.4*	0.21	32
11.0	0.16	41
17.4*	0.10	62

Where (*) Values of Beam Energy (keV) estimated in Reference [51]

Table A2. *Table of Atomic Radii.*

Atomic Number	Element Symbol	Atomic Radius [Å]	Ionic Radius [Å]	Covalent Radius [Å]	Van-der-Waals Radius [Å]	"Crystal" Radius [Å]
22	Ti	1.76	1.40	1.36	"------"	0.75

Source: http://www.crystalmaker.com/support/tutorials/atomic-radii/

References

[1] L. Valgas de Souza. Filmes de ormosils contendo polioxometalatos e seu fotoreatividade frente a lipídeos e proteínas de adesão. 2014.130f. Tese de Doutorado em Físico-Química- Instituto de Química de São Carlos. São Carlos, São Paulo-Brasil: Universidade de São Paulo (IQSC-USP), 2014. Unpublished.

[2] Hench, L., West J. The Sol-Gel Process. Chem. Rev. 1990. 90 (1): 33–72. https://doi.org/10.1021/cr00099a003.

[3] J. Steed, J. Atwood. Supramolecular Chemistry, 2nd Edition. February 2009, 1216 pages ISBN: 978-0-470-51234-0.

[4] Ajay Kumar Manna, "Supramolecular Chemistry-Concepts and Applications", International Journal of Science and Research (IJSR). 2015. 4 (4): 892-899. https://www.ijsr.net/get_abstract.php?paper_id=29031502

[5] Jean-Marie Lehn. "Supramolecular Chemistry-Scope and Perspectives. Molecules-Supermolecules-Molecular Devices". Nobel lecture, December 8, 1987. Angewandte Chemie. 1988. 27 (1): 89-112. https://doi.org/10.1002/anie.198800891

[6] Resnati G, Boldyreva E, Bombicz P, Kawano M. Supramolecular interactions in the solid state. IUCrJ. 2015. 2 (6): 675–690. ISSN: 2052-2525 http://dx.doi.org/10.1107/S2052252515014608 6

[7] Guido Kickelbick (2007). Hybrid Materials: Synthesis, Characterization, and Applications. Wiley-VCH Verlag GmbH & Co. KGaA. Print ISBN: 9783527312993, DOI: 10.1002/9783527610495.

[8] O. A. Elguera Ysnaga. Métodos de Análise de Materiais Híbridos: Um Estudo Comparativo Entre Fluorescência de Raios-X Com Detecção Dispersiva em Energia Usando Fonte Tradicional e Luz Síncrotron. [Doctor of Science in Analytical and Inorganic Chemistry, Thesis]. Instituto de Química de São Carlos. São Carlos, São Paulo-Brasil: Universidade de São Paulo (IQSC-USP), 2015. Pp. 159-163. Unpublished.

[9] L. P. Gonçalves. Nanopartículas de Titânio como aditivos em materiais híbridos inorgânicos fotocrômicos baseados em fosfotungstatos. 2011.138f. Dissertação de Mestrado (Mestrado em Engenharia de Materiais) -Instituto de Química de São Carlos. São Carlos, São Paulo-Brasil: Universidade de São Paulo (IQSC-USP), 2011. Unpublished.

[10] L. Gonçalves, E. Ferreira-Neto, S. Ullah, et al. "Enhanced Photochromic Response of Ormosil–Phosphotungstate Nanocomposite Coatings Doped with TiO_2 Nanoparticles". J. Sol-Gel Sci. Technol. 2015. 76 (2): 386–394. DOI 10.1007/s10971-015-3787-0, Online ISSN 0928-0707, Publisher: Springer US.

[11] Baoling, W.; Hu, L. "Study of hybrid TiO_2/ormosil films doped with laser dyes". Journal of Molecular Structure. 2005. 748 (1–3): 177-181. ISSN 0022-2860. https://doi.org/10.1016/j.molstruc.2005.03.029

[12] Shyam Tripathi, V.; Babu Kandimalla, V.; Ju, H. "Preparation of ormosil and its applications in the immobilizing biomolecules". Sensors and Actuators B: Chemical. 2006. 114 (2): 1071–1082. ISSN0925-4005. https://doi.org/10.1016/j.snb.2005.07.037.

[13] Laranjo, M.; Stefani, V.; Benvenutti, E.; Costa, T.; Ramminger, G.; Gallas, M. "Synthesis of ormosil silica/rhodamine 6G: Powders and compacts. Journal of Non-Crystalline Solids". 2007. 353 (1): 24-30. DOI: 10.1016/j.jnoncrysol.2006.09.029. ISSN 0022-3093.

[14] F. Silva De Carvalho. Efeito da Matriz no Comportamento Fotocrômico de Ormosils de Fosfotungstato. 2008.104f. Dissertação de Mestrado (Mestrado em Ciências (Físico-Química)) – Instituto de Química de São Carlos. São Carlos, São Paulo-Brasil: Universidade de São Paulo (IQSC-USP), 2008. Unpublished.

[15] De Oliveira, M., Lopes de Souza, A., Rodrigues Filho, U. P., Schneider, J. "Local Structure and Photochromic Response in Ormosils Containing Dodecatungstophosphoric Acid". Journal of Materials Chemistry, 23 (4): 953-963, 2011. https://doi.org/10.1021/cm1022272

[16] Heng, H., Gan, Q., Meng, P., Liu, X. "The visible-light-driven type III heterojunction $H_3PW_{12}O_{40}/TiO_2$-In_2S_3: A photocatalysis composite with enhanced photocatalytic activity". Journal of Alloys and Compounds. 2017. 696: 51-59. ISSN 0925-8388. https://doi.org/10.1016/j.jallcom.2016.11.116.

[17] Yao, F., Fu, W., Ge, X., Wang, L., Wang, J., Zhong, W. "Preparation and characterization of a Copper phosphotungstate/Titanium dioxide (Cu-$H_3PW_{12}O_{40}/TiO_2$) composite and the photocatalytic oxidation of high-concentration ammonia nitrogen", Science of The Total Environment. 2020. 727: 138425, ISSN 0048-9697, https://doi.org/10.1016/j.scitotenv.2020.138425.

[18] Rengifo-Herrera, J., Blanco, M., Wist, J., Florian, P., Pizzio, L. "TiO_2 modified with polyoxotungstates should induce visible-light absorption and high photocatalytic activity through the formation of surface complexes". Applied Catalysis B: Environmental, 2016. 189 (1): 99-109, ISSN 0926-3373, https://doi.org/10.1016/j.apcatb.2016.02.033.

[19] Orlando Elguera Ysnaga. "Maser-rays Based on Synchrotron Radiation-Total Reflection X-ray Fluorescence (SR-TXRF)". Engineering Physics. 2021. 5 (2): 40-53. doi: 10.11648/j.ep.20210502.13.

[20] Klockenkämper, R., Von Bohlen, A. "Survey of sampling techniques for solids suitable for microanalysis by Total-Reflection X-ray Fluorescence Spectrometry". J. Anal. At. Spectrom. 1999. 14 (4): 571–576. https://doi.org/10.1039/A807693F

[21] Compton, A. "CXVII. The Total Reflection of X-Rays". Philosophical Magazine Series 1, vol. 45, p1121-1131, 1923.

[22] Parratt, L. G. "Surface Studies of Solids by Total Reflection of X-rays". Physical Reviews. 1954. 95 (2): 359-369. https://link.aps.org/doi/10.1103/PhysRev.95.359.

[23] Yoneda, Y; Horiuchi, T. "Optical flats for use in X-ray Spectrochemical Microanalysis". The Review of Scientific Instruments: 1971. 42 (7): 169-70. https://doi.org/10.1063/1.1685282

[24] Wobrauschek, P; Aiginger, H. "Total-Reflection X-ray Fluorescence Spectrometric Determination of Elements in Nanogram Amounts". Analytical Chemistry. 1975.47 (6): 852–855. https://doi.org/10.1021/ac60356a034

[25] Ladisich, W.; Rieder, R.; Wobrauschek, P.; Aiginger, H. "Total Reflection X-ray Fluorescence analysis with monoenergetic excitation and full spectrum excitation using rotating anode X-ray tubes". Nuclear Instruments and Methods in Physics Research Section A: Accelerators, Spectrometers, Detectors and Associated Equipment. 1993. 330 (3): 501-506. ISSN 0168-9002. https://doi.org/10.1016/0168-9002(93)90582-3

[26] R. Klockenkämper, A. Von Bohlen. "Efficiency and Evaluation". In: M. F. Vitha, editor. Total Reflection X-ray Fluorescence Analysis and Related Methods. New York: John Wiley, 1997. Chap. 6, Pp. 221–230.

[27] R. Klockenkämper, A. Von Bohlen. "Efficiency and Evaluation". In: M. F. Vitha, editor. Total Reflection X-ray Fluorescence Analysis and Related Methods. New York: John Wiley, 2015. Chap. 7, Pp. 434-438.

[28] Pérez, C., Radtke, M., Sánchez, H., Tolentino, H., Neuenshwander, R., Barg, W., Rubio, M., Silveira Bueno, M., Raimundo, I., Rohwedder. "Synchrotron radiation X-Ray fluorescence at the LNLS: beamline instrumentation and experiments". X-ray Spectrometry. 1999. 28 (5): 320–326. https://doi.org/10.1002/(SICI)1097-4539(199909/10)28:5<320::AID-XRS359>3.0.CO;2-1

[29] Elguera Ysnaga Orlando. "Grazing Incidence and Total Reflection X-ray Fluorescence Analyses of Ormosil Thin Films". LNLS 2013 Activity Report. Brazilian Synchrotron Light Laboratory. 2013.

[30] F. Y. Xie, L. Gong, X. Liu, Y. T. Tao, W. H. Zhang, S. H. Chen, H. Meng, J. Chen. "XPS studies on surface reduction of tungsten oxide nanowire film by Ar^+ bombardment". Journal of Electron Spectroscopy and Related Phenomena. 2012. 185 (3–4): 112-118, ISSN 0368-2048. https://doi.org/10.1016/j.elspec.2012.01.004

[31] H. Zhang, C. Cheng, H. Zhang, R. Chen, B. Huang, H. Chen, W. Peiab. "Physical mechanism for the synapse behavior of WTiOx-based memristors". Phys. Chem. Chem. Phys. 2019. 21 (42): 23758-23763. https://doi.org/10.1039/C9CP05060D.

[32] Breckenridge, R., Hosler, W. "Electrical Properties of Titanium Dioxide semiconductors". Phys. Rev. 1953. 91 (4): 793-802. doi = {10.1103/PhysRev.91.793}. https://link.aps.org/doi/10.1103/PhysRev.91.793.

[33] Becker, K. H., Haaks, D. and Schürgers, M. "Notizen: Fluorescence by the Vacuum-UV Photolysis of Acetylene". Zeitschrift für Naturforschung A, 1971, 26 (10): 1770-1771. https://doi.org/10.1515/zna-1971-1031.

[34] Jiang, J., Saladrigas, C., Erickson, T., Keenan, C., Field. R. "Probing the predissociated levels of the S1 state of acetylene via H-atom fluorescence and photofragment fluorescence action spectroscopy". J Chem Phys. 2018 Nov 7; 149 (17): 174309. https://doi.org/10.1063/1.5045046

[35] Brus, L. "Acetylene fluorescence". Journal of Molecular Spectroscopy. 1979.75 (2): 245-250. ISSN 0022-2852. https://doi.org/10.1016/0022-2852(79)90120-6.

[36] Cuylle, S., Zhao, D., Strazzulla, G., Linnartz, H. "Vacuum ultraviolet photochemistry of solid acetylene: a multispectral approach". Astronomy & Astrophysics. 2014. 570, A&A, A83. DOI: 10.1051/0004-6361/201424379. https://doi.org/10.1051/0004-6361/201424379

[37] Okabe, H. "Photochemistry of acetylene". 1983, Can. J. Chem. 61, 850-855. https://doi.org/10.1139/v83-153.

[38] Kočišek, J., Fedor, J., Poterya, V., Pysanenko, A., O. Votava, M. Fárník. "UV Photodissociation of Acetylene in Various Environments". WDS'11 Proceedings of Contributed Papers, Part II, 241–246, 2011. ISBN 978-80-7378-185-9 © MATFYZPRESS.

[39] Tanimoto, H., Nagao, T., Fujiwara, T., Kakuta, T., Tanaka, K., Chujo, Y. and Kakiuchi, K. "Fluorescence and phosphorescence study of germanium–acetylene polymers and germa [N] pericyclynes". Polym. Chem., 2015, 6 (43) 7495-7499.

[40] Byzynski, G., Ribeiro, C., Longo, E. "Blue to Yellow Photoluminescence Emission and Photocatalytic Activity of Nitrogen Doping in TiO_2 Powders". International Journal of Photoenergy. 2015. Volume 2015, Article ID 831930, 12 pages. https://doi.org/10.1155/2015/831930. https://doi.org/10.1155/2015/831930DO

[41] Liu, Y., Claus, R. O. "Blue Light Emitting Nanosized TiO_2 Colloids". J. Am. Chem. Soc. 1997, 119 (22): 5273–5274. https://doi.org/10.1021/ja970587q

[42] Hayyan, M., Hashim, M., AlNashef, I. "Superoxide Ion: Generation and Chemical Implications". DOI: 10.1021/acs.chemrev.5b00407 Chem. Rev. 2016, 116, 5, 3029−3085. https://doi.org/10.1021/acs.chemrev.5b00407

[43] Mayeda, E. A., Bard, A. J. "Singlet oxygen. Suppression of its production in dismutation of superoxide ion by superoxide dismutase". J. Am. Chem. Soc. 1974, 96 (12): 4023–4024. https://doi.org/10.1021/ja00819a054

[44] Zent, A., Ichimura, A., Quinn, R., Harding, H. "The formation and stability of the superoxide radical (O_2^-) on rock-forming minerals: Band gaps, hydroxylation state, and implications for Mars oxidant chemistry". Journal of Geophysical Research, Vol. 113, E09001, 2008. https://doi.org/10.1029/2007JE003001

[45] Farley J, Hough S (2003). "Single Bubble Sonoluminsescence". APS Northwest Section Meeting Abstracts: D1.007.

[46] Frenzel, H. and Schultes, H. "Luminescenz im ultraschallbeschickten Wasser". Zeitschrift für Physikalische Chemie International Journal of Research in Physical Chemistry and Chemical Physics. 1934. 27B (1): 421-424. https://doi.org/10.1515/zpch-1934-2737. Published Online: 2017-01-12.

[47] Didenko Y, McNamara W, Suslick K. "Effect of Noble Gases on Sonoluminescence Temperatures during Multibubble Cavitation". Physical Review Letters. 2000, 84 (4): 777–780.

[48] Jarman, P. "Sonoluminescence: A discussion". The Journal of the Acoustical Society of America. 1960, 32 (11): 1459–1462. ISSN 0001-4966. doi: 10.1121/1.1907940.

[49] Suslick, K. "The chemical effects of ultrasound," Scientific American, 1989, 260 (2), 80-86.

[50] A Star in a Jar!..... SOUND Can Produce LIGHT..... Sonoluminescence. https://steemit.com/steemstem/@physics.benjamin/sound-can-produce-light-a-star-in-a-jar-sonoluminescence

[51] Klockenkämper, R. Total Reflection X-ray Fluorescence Analysis. Chemical analysis A series of monographs on analytical chemistry and its applications, v. 140, New York: John Wiley, 1997. 246 p.

[52] F. F. Beijer. (1998). "Cooperative Multiple Hydrogen Bonding in Supramolecular Chemistry". ISBN 90-386-0698-2. Cip-Data Library Technische Universiteit Eindhoven.

[53] Egerton, T., Purnama, H. "Does hydrogen peroxide really accelerate TiO_2 UV-$_C$ photocatalyzed discoloration of azo-dyes such as Reactive Orange 16?". Dyes and Pigments. 2014. 101: 280-285. ISSN: 0143-7208. DOI: 10.1016/j.dyepig.2013.10.019.

[54] D. Huang, Y. Wang, L. Yang, G. Luo. "Direct synthesis of mesoporous TiO_2 modified with phosphotungstic acid under template-free condition". Microporous and Mesoporous Materials. 2006. 96 (1–3): 301–306. ISSN 1387-1811, https://doi.org/10.1016/j.micromeso.2006.06.040.

[55] Javidi, J., Esmaeilpour, M., Rahiminezhad, Z. et al. "Synthesis and Characterization of $H_3PW_{12}O_{40}$ and $H_3PMo_{12}O_{40}$". Nanoparticles by a Simple Method. J Clust Sci. 2014. 25: 1511–1524. https://doi.org/10.1007/s10876-014-0745-x

[56] Zhou, Y., Yang, J., Su, H., Zeng, J., Ping-Jiang, S., Goddard. W. "Insight into Proton Transfer in Phosphotungstic Acid Functionalized Mesoporous Silica-Based Proton Exchange Membrane Fuel Cells". Journal of the American Chemical Society. 2014. 136 (13): 4954-4964. https://doi.org/10.1021/ja411268q.

[57] Liu, Y., Lu, Y., Haragirimana, A., Buregeya, I., Li, N., Hu, Z., Chen, S. "Immobilized phosphotungstic acid for the construction of proton exchange nanocomposite membranes with excellent stability and fuel cell performance". International Journal of Hydrogen Energy. 2020. 45 (35): 17782-17794. ISSN 0360-3199. https://doi.org/10.1016/j.ijhydene.2020.04.159.

[58] Ternov, I. M. Synchrotron Radiation and Its Applications. Translated from Russian by S. J. Amoretty. New York: Harwood Academic Publishers, 1985. 379p.

1 In order to reduce the dead time of the measurements and to minimize the absorption of the fluorescent X-ray emission of the cations (auto-absorption effect) [8].

2 [http://www.silx.org/doc/PyMca/dev/index.html]

3Also is observed two peaks at 10 keV and 11 keV approximately, corresponding to the Compton and Rayleigh scattering peaks respectively.

4At incident angles 0.06° and 0.10° of SR-XRF beam, the TXRF condition are met for ormosil films [8, p. 161].

5 At ormosil films the average rugosity is at range 0.1-10 Å <> 0.01-1nm [1, 8], which are less than the estimated depths of the Total Reflection condition (27-41nm) [8 p. 161, 33, 34]. For this reason, it is feasible the TXRF analysis.